FOSSIL ENERGY

NIPER-431
(DE90000205)

GAS MISCIBLE DISPLACEMENT

Foams For Mobility Control and Improvement In Gas Sweep Efficiency

Topical Report

By
Feliciano M. Llave
Frank T. H. Chung
Randall W. Louvier
David A. Hudgins

December 1989

Performed Under Cooperative Agreement No. FC22-83FE60149

IIT Research Institute
National Institute for Petroleum and Energy Research
Bartlesville, Oklahoma

Bartlesville Project Office
U. S. DEPARTMENT OF ENERGY
Bartlesville, Oklahoma

This report has been reproduced directly from the best available copy.

Available to DOE and DOE contractors from the Office Of Scientific and Technical Information, P.O. Box 62, Oak Ridge, TN 37831; prices available from (615)576-8401, FTS 626-8401.

Available to the public from the National Technical Information Service, U.S. Department of Commerce, 5285 Port Royal Rd., Springfield, VA 22161

Price: Printed A04
Microfiche A01

NIPER-431
Distribution Category UC-122

GAS MISCIBLE DISPLACEMENT
Foams for Mobility Control and Improvement in Gas Sweep Efficiency

Topical Report

By
Feliciano M. Llave
Frank T. H. Chung
Randall W. Louvier
David A Hudgins

December 1989

Work Performed Under Cooperative Agreement No. FC22-83FE60149

Prepared for
U.S. Department of Energy
Assistant Secretary for Fossil Energy

Jerry Casteel, Project Manager
Bartlesville Project Office
P.O. Box 1398
Bartlesville, OK 74005

Prepared by
IIT Research Institute
National Institute for Petroleum and Energy Research
Box 2128
Bartlesville, OK 74005

TABLE OF CONTENTS

Page

Abstract 1
Introduction 2
Acknowledgments 5
Foam Flow Behavior in Smooth Capillary Tubes and Packed Glass Tubes 5
  Experimental Apparatus 5
  Experimental Procedure 8
  Experimental Results and Discussion 9
    Fluid Flow in Capillary Tubes 9
    Foam Behavior in Smooth Capillary Tubes 10
    Foam Behavior in Packed Glass Tubes 19
    Comparison Calculations Using Predictive Model for Foam Apparent Viscosity 29
  Effect of Injection Rate on Foam Performance 36
  Effect of Foam on Gas Sweep Improvement and Gas-Water Relative Permeability 40
    The Effectiveness of Foam for Gas Sweep Improvement 40
    Experimental Apparatus and Procedure 40
    Experimental Results and Discussion 40
  Effect of Foam on Gas-Water Relative Permeabilities 44
    Experimental Apparatus and Procedure 44
    Experimental Results and Discussion 46
Summary 51
  Foam Flow Behavior in Smooth and Packed Capillary Tubes 51
  Effect of Injection Rate on Foam Performance 52
  Effect of Foam on Gas Sweep and Gas-Water Relative Permeability 52
References 53

TABLES

1. Capillary tube assembly characteristics 7
2. Measured apparent viscosity in the smooth capillary tube assembly 20
3. Measured apparent viscosity in the packed glass tube assembly 30
4. Experimental parameters used in the predictive model calculations 32
5. Experimental parameters for gas-liquid relative permeability measurements 45
6. Results of relative permeability measurements 46

ILLUSTRATIONS

Page

1. Outline of modeling foam flow in porous media. 3
2. Schematic diagram of foam apparent viscosity apparatus. 6
3. Measured surface tension versus surfactant concentration....11
4. Apparent viscosity versus shear rate and foam quality for nitrogen + 2 wt % Alipal CD-128 in DIW at room temperature....11
5. Flow rate versus differential pressure per unit length for nitrogen + 2 wt % Alipal CD-128 in DIW at room temperature....12
6. Apparent viscosity versus shear rate for nitrogen + 2 wt % Alipal CD-128 in DIW at room temperature. 12
7. Apparent viscosity versus shear rate and foam quality for nitrogen + 0.5 wt % Alipal CD-128 in DIW at room temperature. 13
8. Flow rate versus differential pressure per unit length for nitrogen + 0.5 wt % Alipal CD-128 in DIW at room temperature....13
9. Apparent viscosity versus shear rate for nitrogen + 0.5 wt % Alipal CD-128 in DIW at room temperature. 14
10. Apparent viscosity versus shear rate and foam quality for nitrogen + 0.5 wt % Alipal CD-128 in DIW at 50° C. 15
11. Flow rate versus differential pressure per unit length for nitrogen + 0.5 wt % Alipal CD-128 in DIW at 50° C. 16
12. Apparent viscosity versus shear rate for nitrogen + 0.5 wt % Alipal CD-128 in DIW at 50° C. 16
13. Frequency distribution of ratio of bubble radius to tube radius for nitrogen + 0.5 wt % Alipal CD-128 in DIW at room temperature....17
14. Foam bubble size ratio versus shear rate and foam quality for nitrogen + 0.5 wt % Alipal CD-128 in DIW at 50° C....18
15. Comparison of foam bubble size ratio versus shear rate and foam quality for nitrogen + 0.5 wt % Alipal CD-128 in DIW at room temperature and 50° C....18
16. Apparent viscosity versus gas velocity and foam quality for nitrogen + 2 wt % Alipal CD-128 in DIW at room temperature....23
17. Apparent viscosity versus gas velocity for nitrogen + 2 wt % Alipal CD-128 in DIW at room temperature. 23
18. Resistance factor versus total flow rate and foam quality for nitrogen + 2 wt % Alipal CD-128 in DIW at room temperature. 25

ILLUSTRATIONS -- Continued

Page

19. Mobility reduction versus gas velocity for nitrogen + 2 wt % Alipal CD-128 in DIW at room temperature. 25
20. Foam bubble size ratio versus foam quality in the inlet section of the packed tube assembly....26
21. Foam bubble size ratio versus foam quality in the packed section of the packed tube assembly....27
22. Foam bubble size ratio versus foam quality in the outlet section of the packed tube assembly....27
23. Foam bubble size ratio versus foam quality in the inlet section of the packed tube assembly at a shear rate of 5.03 sec^{-1}. 28
24. Foam bubble size ratio versus foam quality in the inlet section of the packed tube assembly at a shear rate of 10.06 sec^{-1} 28
25. Foam bubble size ratio versus foam quality in the inlet section of the packed tube assembly at a shear rate of 25.15 sec^{-1}. 29
26. Comparison of predicted and measured apparent viscosity versus foam quality in smooth capillary tubes....32
27. Comparison of measured apparent viscosity versus foam quality for nitrogen + 2 wt % Alipal CD-128. 34
28. Comparison of predicted and measured apparent viscosity versus ratio of r_B/R in smooth capillary tubes....34
29. Comparison of predicted and measured apparent viscosity versus gas velocity in packed glass tubes....35
30. Coreflood no. 1: Nitrogen displacing brine at 50 cm^3/hr. 38
31. Coreflood no. 2: Nitrogen displacing surfactant solution at 5 cm^3/hr....38
32. Coreflood no. 3: Nitrogen displacing surfactant solution at 50 cm^3/hr....39
33. Effect of injection rate on foam generation....39
34. Dual-core foam flood apparatus....41
35. Gas mobility history of dual-core foam flood #1: cores vertical. 41
36. Gas mobility history of dual-core foam flood #2: cores horizontal....43
37. Gas mobility history of dual-core foam flood #3: cores horizontal....43
38. Gas mobility history of dual-core foam flood #4: cores vertical. 44
39. Gas-/water relative permeability test no. 2, using foamer at 6.1 psi/ft in a low-permeability core....47

ILLUSTRATIONS -- Continued

Page

40. Gas-water relative permeability test no. 3, using brine at 6.1 psi/ft in a low-permeability core. 47
41. Gas-water relative permeability test no. 4, using foamer at 2.5 psi/ft in a high-permeability core...48
42. Gas-water relative permeability test no. 5, using foamer at 5.0 psi/ft in a high-permeability core...48
43. Gas-water relative permeability test no. 6, using brine at 5.0 psi/ft in a high-permeability core.....49
44. Gas-water relative permeability test no. 7, using brine at 2.5 psi/ft in a high-permeability core.....49

GAS MISCIBLE DISPLACEMENT

Foams for Mobility Control and Improvement in Gas Sweep Efficiency

by Feliciano M. Llave, Frank T.H. Chung, Randall W. Louvier, and David A. Hudgins

---

ABSTRACT

This report presents the results of experimental studies relating to mobility control and sweep efficiency in gas flooding that were focused on several topics: (1) the study of foam flow behavior in smooth capillary tubes and packed glass tubes; (2) the effect of injection rate on foam performance; and (3) the study of the effect of foam on gas-water relative permeabilities. These studies were conducted to facilitate the understanding of the behavior of foam flow and its potential application in gas flooding processes.

The study of foam flow behavior in smooth capillary tubes and packed glass tubes was designed to observe and quantify the behavior of foam under various experimental conditions. The experimental variables included foam quality, shear rate, surfactant concentration, and temperature. The apparent viscosity, resistance factor, and reduction in the mobility of foam in smooth capillary tubes and packed glass tubes were measured. The bubble size distribution of pregenerated foam was measured to determine the contribution of foam texture to its flow behavior. A comparison of the experimental results was made using available mathematical models developed for predicting foam apparent viscosities in smooth capillary tubes and packed glass tubes. The measured apparent viscosity in the smooth capillary tubes showed no significant dependence on surfactant concentration above the critical micellar concentration (CMC) of the system, but was slightly dependent on the temperature conditions. The foam quality altered the behavior of the foam. Foam qualities greater than 75% exhibited considerably different behavior than foam at lower qualities. Observations on foam bubbles sizes showed significantly larger foam bubbles were present at higher foam qualities, however, an increase in shear rate corresponded to a decrease in a foam bubble size.

Several coreflooding experiments were conducted to determine the effect of injection rate on foam generation and performance and the effect of the presence of foam on gas-water relative permeability. Constant-pressure coreflooding studies using dual, parallel cores provided an opportunity for using foam to divert gas flow from high-permeability zones to unswept lower-permeability zones, thereby increasing overall sweep efficiency and oil recovery. Using single cores, gas-water relative permeabilities were measured to determine the effects of foam. Foam was not considered as a separate flowing phase; instead, it was found that flow calculations can be simplified by treating the foamer as the water phase and experimentally measuring the resulting relative permeabilities.

INTRODUCTION

Gas flooding as an enhanced oil recovery (EOR) process involves the injection of specific gases to produce oil that would not be recovered otherwise.[1] Gas flooding displacement efficiency can be economically feasible under both miscible and immiscible conditions.[2] The efficiency of these processes has been hindered by the unfavorable mobility of the injected gas as well as gravity segregation, which result in poor sweep efficiency. The basic contributing factors to these problems are the low density and viscosity of the gas at reservoir conditions. Several methods have been considered to mitigate the problem of mobility control: (1) a water-alternating gas (WAG) process; (2) use of surfactants to generate foam to reduce gas mobility; (3) viscosifying the gas phase by means of addition of polymers as direct thickeners[3-4] and (4) in situ polymerization of soluble monomers in supercritical CO_2.[5] A method utilizing entrainers that are soluble in CO_2 was developed at NIPER to enhance the extraction power of the CO_2-rich phase and enhance the viscosity and density of the gas phase. Preliminary tests based on this concept have shown encouraging results,[6-7] and further research is on-going to develop this method. This report will deal specifically with the method of utilizing surfactants to generate foams for gas mobility control.

Interest in the use of foams has resulted from their potential application as mobility control agents for improving oil recovery in EOR processes. A considerable number of technical papers have been published on studies of foam behavior in porous media. Studies on using foams for mobility control have also been directed towards their use in steamflooding and solvent flooding as well as displacement processes using CO_2 or other gas.[8-18] However, most of the papers deal only with phenomenological descriptions of foam behavior in laboratory coreflood tests and effectiveness in gas mobility control. Several mathematical models that can to some degree predict foam generation and propagation in porous media have been developed. Although foam applications have been successfully tested in laboratory studies, the application of foam in EOR is still in its primary stages, primarily because of the lack of adequate models or scaling rules to describe its behavior. Research is needed on the development of quantitative relationships of foam behavior, rather than qualitative descriptions. Some progress in the development of prototype models describing foam behavior has been made.[19-20] Figure 1 illustrates the modeling hierarchy. The model in figure 1 employs Darcy's equation with modifications introduced in terms describing relative permeability and viscosity of foam in porous media. This simplified approach provides a framework to develop a model that is computationally convenient and useful. Darcy's equation continues to be the equation of choice within the petroleum engineering field for describing multiphase flow in porous media. Both the apparent foam viscosity and the effective gas relative permeability depend on foam texture. The bubble size distribution, or equivalently the foam texture is a controlling factor for the rheological properties of foam in porous media. Some correlations for the apparent foam viscosity and

gas relative permeability have been presented.[20-22] A simple one-dimensional foam population-balance model has been developed to quantify the foam texture behavior. The number density of the foam bubbles or lamellae is dependent on the mechanisms of generation and coalescence of these bubbles. The mechanisms of foam generation and coalescence is then dependent on surfactant concentration, capillary pressure, gas flow rate, and pore structure.[23-27] The adsorption of the surfactant comes into play in the mass balance equation for the surfactant. the mass balance equation in turn dictates the availability of the surfactant to generate foam. As is shown in figure 1, many relationships such as the dependence of foam viscosity on foam characteristics need to be developed. This present work is designed to contribute to developments of correlations for foam apparent viscosity and effective foam relative permeability.

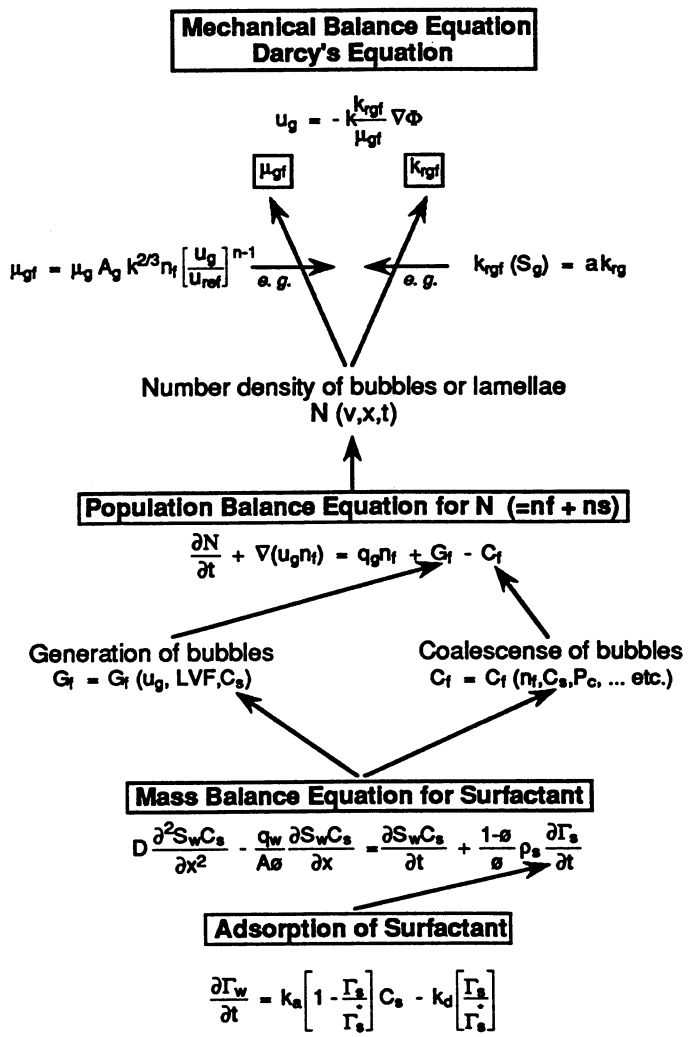

FIGURE 1. - Outline of modeling foam flow in porous media.

The complexity of foam flow in porous media necessitates the study of its behavior under conditions involving simpler constraints. Flow in smooth capillary tubes without oil present provides approximate conditions that are far simpler than those in porous media where different factors such as tortuosity, multiple phase saturations, reservoir heterogeneity, and other factors must be considered. Studying the behavior of foam in smooth capillary tubes and packed glass tubes is based on the approach of approximating flow in porous media as fluid flow in a bundle of capillary tubes. Hirasaki and Lawson[21] have investigated the behavior of foam flow in smooth capillaries. The apparent viscosity of foam flowing in smooth capillaries was measured experimentally, and a mathematical model was developed to predict the apparent viscosity of foam under different conditions. Their study attributed foam texture as a key parameter in the determination of foam flowing through a capillary. The work of Falls et al.[22] adds a greater degree of complexity to the study of foam by investigating the effect of pore constrictions on foam flow behavior in homogeneous bead packs. The mobilities of aqueous foams of known texture were measured, and the theory describing apparent viscosity of foams in smooth capillaries was extended to account for several factors inherent in flow in porous media. These studies are representative of the amount of research and attention that has been focused on understanding the behavior of foam for the purpose of the development of the necessary technology for its successful utilization in EOR applications. They represent major steps towards developing a good description of the behavior of foam in porous media in reservoir formation. The behavior of foam flow is even more complicated and is rather unpredictable. Gaps in understanding of foam behavior can be seen in laboratory studies that have shown successful experiments in utilizing foam while field tests that have fallen short of expectations.[28]

This project was focused on several areas: (1) the study of foam flow behavior in smooth capillary tubes and packed glass tubes; (2) the effect of injection rate on foam performance; and (3) the study of the effect of foam on gas-water relative permeabilities and improving sweep efficiency. In the study of foam flow behavior, an apparatus was designed and constructed to observe the behavior of foam and to measure apparent viscosity under different conditions. A comparison of the experimental results was also made using theoretical models developed for predicting foam apparent viscosities in smooth capillaries and packed glass tubes.[21-22] The surfactant used for the study was Alipal CD-128, manufactured by GAF Corporation. It is an ammonium salt of ethoxylated and sulfated decyl and octyl alcohols. The surfactant samples are received as 56% active, containing 13% ethanol and 31% water. The experiments were not designed to select the best foaming agent, but rather to utilize a foaming agent that had been studied extensively and discussed in the literature.[29-30] This part of the project represents a step towards providing more information regarding the behavior of foam flow under less restrictive constraints.

The second area of study, that of the effect of foam on gas sweep efficiency, and gas-water relative permeabilities, was conducted using two different sets of experiments which used the same apparatus.

Gas sweep efficiency improvements were studied in dual, parallel core experiments. Slugs of foamer were injected into the cores and allowed to go where they would and divert gas flow from a high-permeability core to a low-permeability one, much as happens within different zones or layers in a reservoir. Single-core experiments measured the effect of foamer upon gas-water relative permeabilities by the unsteady-state method, wherein gas displaced the water. Sequential tests were run where the fluid initially saturating the rock was brine in one test and foamer in the second test. Core absolute permeabilities and pressure differentials across the core were varied one at a time to quantify their effect on the relative permeabilities. For the same purpose explained previously, the Alipal CD-128 surfactant solution was used as the foamer.

ACKNOWLEDGMENTS

This work was sponsored by the U.S. Department of Energy under cooperative agreement DE-FC22-83FE6-0149. The authors wish to thank Dr. Thomas E. Burchfield of NIPER for his helpful advice and support during the course of the study and GAF Corporation for providing the surfactant samples used in the study.

FOAM FLOW BEHAVIOR IN SMOOTH CAPILLARY TUBES AND PACKED GLASS TUBES

Experiments were conducted to determine foam flow behavior in smooth capillary tubes and glass tubes packed with glass beads. Of primary interest in the study was the observation of the flow behavior of foam under different experimental conditions. Experimental variables that were considered included foam quality, shear rate, surfactant concentration, and temperature. The objective of this study was to measure the apparent viscosity and the resistance factor of foam in smooth capillary tubes and packed glass tubes. Bubble size distributions of pregenerated foam were measured to determine the contribution of foam texture to its flow behavior. Mathematical models[21-22] developed to describe apparent viscosity in smooth capillary tubes and packed glass tubes were tested with the measurements of foam viscosities conducted in the experimental study.

Experimental Apparatus

An experimental apparatus was designed and built to facilitate measurements of the apparent viscosity and the resistance factor of foam in smooth capillary tubes and packed glass tubes and to provide the capability to visually observe and record the texture of foam and its flow behavior.

The apparatus consisted of direct drive pumps, floating piston vessels, a core plug foam generation assembly with an overburden pressure, a high-pressure sight glass, a capillary tube assembly with pressure taps, a backpressure regulator, and differential pressure transducers and transmitters. A schematic diagram of the apparatus is shown in figure 2. Experiments conducted in smooth and packed

capillary tubes required only the replacement of the capillary tube assembly for each specific experiment. Visual observations of the flow behavior were made and recorded using a video enhanced microscopy apparatus. A computerized data-acquisition system was also incorporated in the design to facilitate monitoring of differential pressures (transducer voltage output) across the capillary tubes.

The characteristics and dimensions of the capillary tubes used in the experiments are listed in table 1. A longer tube was used for the smooth capillary experiments to obtain more accurate measurements of differential pressures during flow conditions. Isco variable-rate direct-drive pumps were used to inject the displacement fluid (water) into two floating piston vessels containing nitrogen and surfactant solution, respectively. Rates of injection were varied to achieve the desired effect in varying gas-to-surfactant ratio. The foam quality variation was achieved by adjusting the ratio of gas-to-surfactant injected. These pumps have a maximum operating pressure of 3,700 psig and a continuously adjustable flow rate from 1.5 to 400.0 cm^3/hr at any rated pressure.

A core plug was used in the apparatus to externally generate foam prior to injection into the capillary tube assembly. The high-permeability core plug was housed inside a Hassler type coreholder.

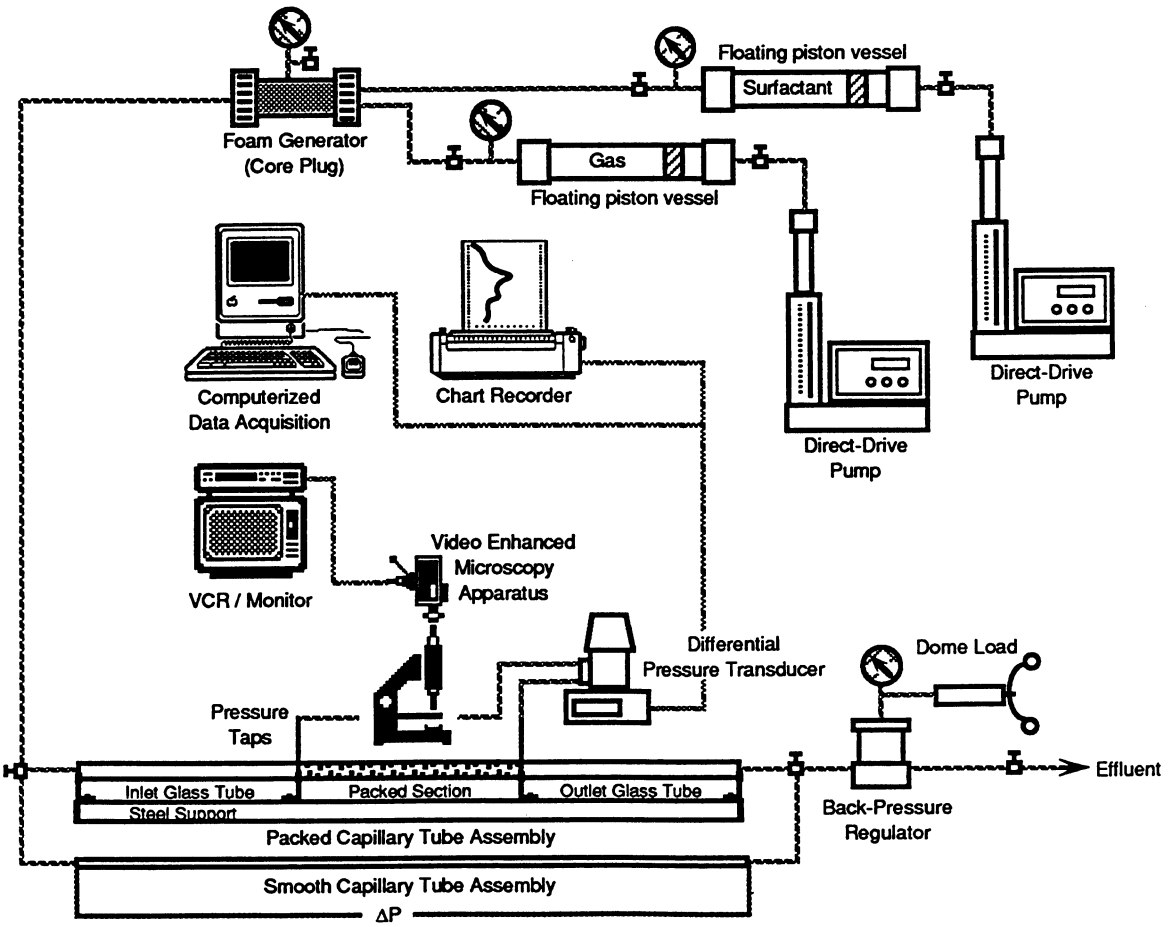

FIGURE 2. - Schematic diagram of foam apparent viscosity apparatus.

TABLE 1. - Capillary tube assembly characteristics

Smooth capillary tube assembly	
Material	stainless steel
Inside diameter, cm	0.228
Length, cm	148.0

Packed glass tube assembly	
Material	glass tube
Inside diameter, cm	0.175
Length, cm	32.0
Packing material	glass beads
Average bead diameter, cm	0.035
Porosity (ø)	0.368
Permeability (k), darcy	105.8

Simultaneous injection of gas and surfactant solution into the core plug resulted in external foam generation prior to injection into the capillary tube. The core plug foam generator produced foam bubbles of a limited range of bubble sizes, of radius less than 0.01 cm. The apparatus was modified to generate larger foam bubbles. Larger bubbles were generated by installing a packed tube after the core plug foam generator. The packed tube was 1 foot long and $^1/_4$ inch OD and was packed with 1-mm glass beads.

The pressure gradient across the smooth capillary assembly was accurately measured using a TOBAR Model 75 DPI differential pressure transmitter, with a maximum differential pressure of 2.17 psi. The maximum operating pressure for this transmitter was 3,375 psig. Signals from the pressure transmitter were read using two Newport Electronic Model Q2000p differential pressure monitors with a display range of 0 to ±1,999 mV. Both the inlet pressure connected to the first pressure tap, and the outlet pressure, before the backpressure regulator, were measured using Heise pressure gauges with a pressure rating of 300 psig. Pressure readings were accurate to within ±0.5 psi. A Fisher Recordall Series 5,000 dual pen chart recorder was used to monitor the output voltage of the differential pressure monitor. This set-up allowed for monitoring the trend or progressive changes in the differential pressure across the capillary. A Temco backpressure regulator was used to maintain flow at a constant backpressure. The

foam flow experiments in packed glass tubes generated higher differential pressures across the packed section. A Validyne differential pressure transducer was used in these experiments. This transducer was rated to a maximum differential pressure of 125 psig. The pressure measurements using this set-up were accurate to ±0.5 psi.

Experimental Procedure

Experiments in smooth capillary tubes and packed glass tubes were conducted in the same manner, except for the difference in applied backpressure for the two experiments. Experiments in smooth capillary tubes were conducted under a constant backpressure of 100 psig, while the experiments in packed glass tubes were conducted under a backpressure of 150 psig. Injection lines and the capillary tube were initially filled with the surfactant solution. The differential pressure across the capillary with the flow of surfactant solution was determined to provide a baseline for the surfactant solution alone. Upon reaching a stable differential pressure reading, the two Isco pumps were adjusted to predetermined flow rates to achieve desired flow rate ratios, while maintaining the same total injection rate as that used in the determination of the surfactant ΔP baseline. Variation of the flow rate ratios corresponded to a variation of the gas-to-surfactant ratio. In these experiments, the foam quality (gas volume/total volume) was varied by adjusting the gas-to-surfactant flow rate ratio. Flow of the initial pregenerated foam was directed through the by-pass section of the capillary assembly. This was necessary to allow the flow rate and texture of the generated foam to stabilize in terms of flow and in terms of texture. Visual observations of the foam flowing through the by-pass tube were made to monitor the consistency and uniformity of the foam bubbles being generated. After some degree of bubble uniformity had been achieved in the foam flowing through the by-pass tube, the flow was then directed through the capillary tube assembly to determine the differential pressure across the tube. The chart recorder was used to monitor dynamic changes in the differential pressure across the capillary tube assembly until a stable reading was achieved. When stable or steady-state conditions were achieved, the computer-controlled, data-acquisition system was used to record the steady-state differential pressure (transducer voltage output) across the capillary. During the course of measuring the steady-state conditions of the experiment, visual observations of the foam bubble texture were made and recorded in video tape to determine foam bubble size distributions under different operating conditions. The experiment was considered completed when measurements of the differential pressure and foam bubble texture recording had been made. The experimental system was then thoroughly flushed with the surfactant solution to eliminate residual foam bubbles in the assembly.

Experimental Results and Discussion

Fluid Flow in Capillary Tubes

Under conditions where a fluid is flowing through a straight horizontal tube of a circular cross section, as in a capillary tube, the shear stress at the tube wall, τ_w, can be expressed as:[31]

$$\tau_w = \frac{R\Delta P}{2L} \tag{1}$$

This equation is valid with the assumption that flow is steady, isothermal, and laminar and that the fluid does not slip at the tube wall. It is expressed as a general relationship that is independent of the nature of the flowing fluid. In this equation, R is the inside radius of the capillary tube, L is the length of tube, and ΔP is the differential pressure across that section of tube.

The viscosity of the fluid, μ, is the ratio of the shear stress, τ, to the shear rate, $\mathring{\gamma}$, expressed as:

$$\mu = \frac{\tau}{\mathring{\gamma}} \tag{2}$$

The value of the rate of shear at the wall, $\mathring{\gamma}_w$, is needed to calculate the fluid viscosity using the shear stress at the tube wall calculated from equation 1. A general expression was derived by Rabinowitsch[32] to describe the shear rate at the wall of the capillary tube. This expression is as follows:

$$\mathring{\gamma}_w = \frac{1}{\pi R^3}\left[3Q + \Delta P \frac{dQ}{d\Delta P}\right] \tag{3}$$

In this equation, Q is the volumetric rate of fluid flow. Using equations 1 through 3, a general equation for the viscosity of the fluid flowing in the tube can be derived.

For Newtonian fluids, equation 3 reduces to:

$$\mathring{\gamma}_w = \frac{4Q}{\pi R^3} \tag{4}$$

with the fluid viscosity expressed as:

$$\mu = \frac{\pi R^4 \Delta P}{8QL} \tag{5}$$

a convenient form of Poiseuille's equation.[33] For power-law fluids, equation 3 reduces to:

$$\mathring{\gamma}_w = \frac{Q}{\pi R^3}\left[\frac{3n+1}{n}\right] \tag{6}$$

where n is the power-law fluid index, with the viscosity expressed as:

$$\mu = \frac{\pi R^4 \Delta P}{2QL} \left[\frac{n}{3n + 1}\right] \tag{7}$$

Foam Behavior in Smooth Capillary Tubes

Experiments were conducted to observe foam flow behavior in smooth capillary tubes. Different experimental variables were considered including foam quality, shear rate, surfactant concentration, and temperature. Apparent viscosities were measured and foam bubble size distributions were observed and measured under different conditions. The range of surfactant concentration used in the experiments was based on the measured critical micellar concentration (CMC) for this system. A plot of the measured surface tension versus surfactant concentration is shown in figure 3. The CMC for the surfactant solution in deionized water was determined to be about 0.10 wt %. Concentrations used in this study were well above the CMC.

Results of experiments conducted at room temperature of 25° C using 2.0 wt % surfactant are presented in figures 4 through 6. Figure 4 shows a three-dimensional (3-D) representation of the measured apparent viscosity as a function of shear rate and foam quality. The plot shows that the apparent viscosity of the foam increased with increasing foam quality. This behavior has been previously observed.[34-35] The plot also shows some dependence of the foam apparent viscosity on shear rate. Figure 5 shows a plot of the total flow rate versus the differential pressure per unit length plotted on a log-log scale. The plot indicates some difference in behavior of the 60% quality foam from that of the ones having qualities greater than 75%. The change in packing configuration of foam would have contributed to this difference. This packing configuration change occurs at 74.1% foam quality, the critical quality resulting from the assumption of foam having a rhombohedral packing configuration.[21] No significant dependence of the apparent viscosity on shear rate can be seen in figure 6. Some indication of a shear thinning behavior can be noted for the 60% foam quality but a slight shear thickening behavior can be observed for systems greater than 75% foam quality. Shear thinning behavior of foam has been observed previously.[34-35]

Results of experiments conducted at room temperature using 0.5 wt % surfactant are shown in figures 7 through 9. Figure 7 shows a 3-D plot of the measured apparent viscosity as a function of shear rate and foam quality. Comparing the results of this experiment with that of the study at 2.0 wt % concentration shows a slightly higher or comparable range of measured apparent viscosities with respect to foam quality and shear rate. Figure 8 shows a plot of the flow rates versus differential pressure per unit length. Difference in behavior of the 60% foam from that of the other experiments was also observed. The slope of the lines varied considerably. The shift from shear thinning to shear thickening behavior is shown in figure 9. The shear thinning behavior shifted to shear thickening behavior at foam quality greater

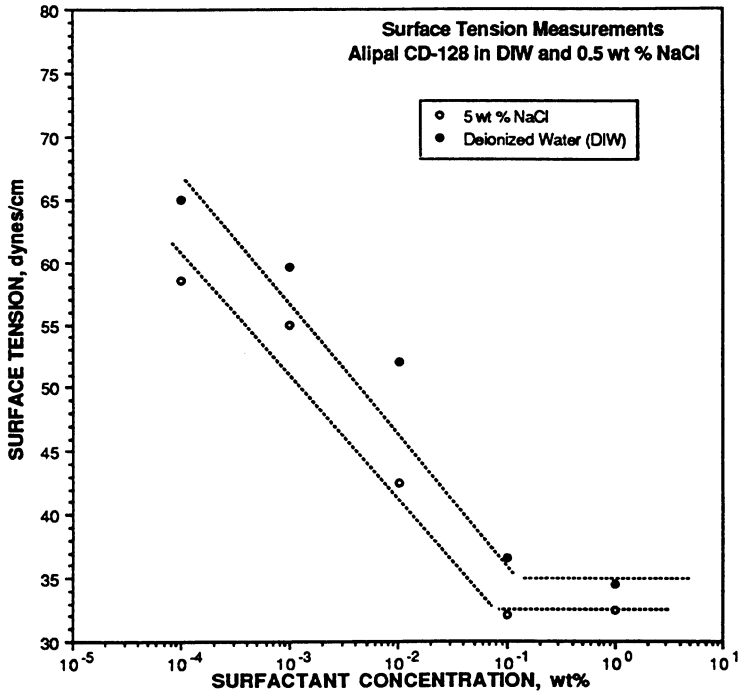

FIGURE 3. - Measured surface tension versus surfactant concentration

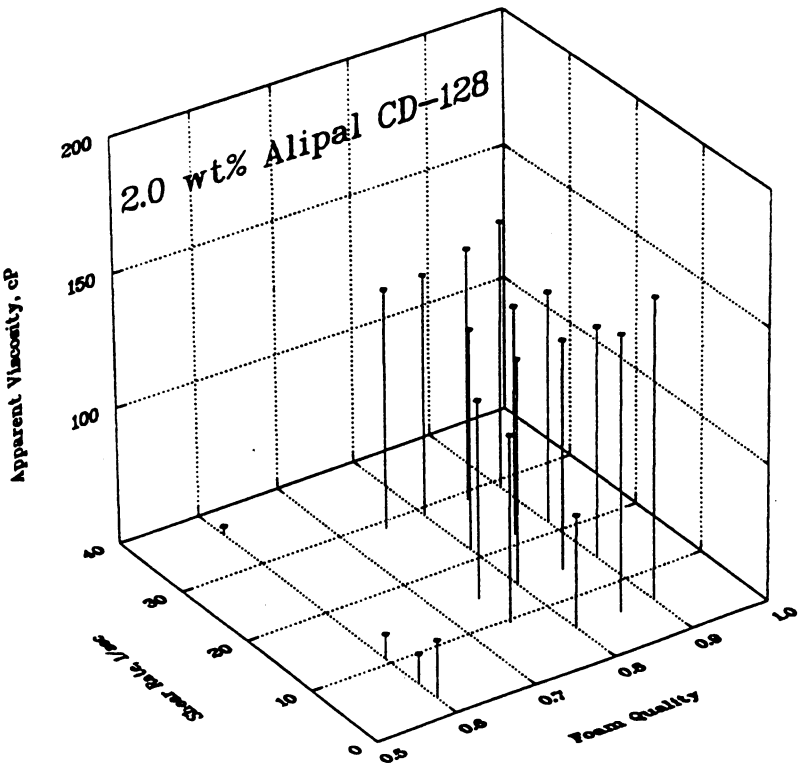

FIGURE 4. - Apparent viscosity versus shear rate and foam quality for nitrogen + 2 wt % Alipal CD-128 in DIW at room temperature.

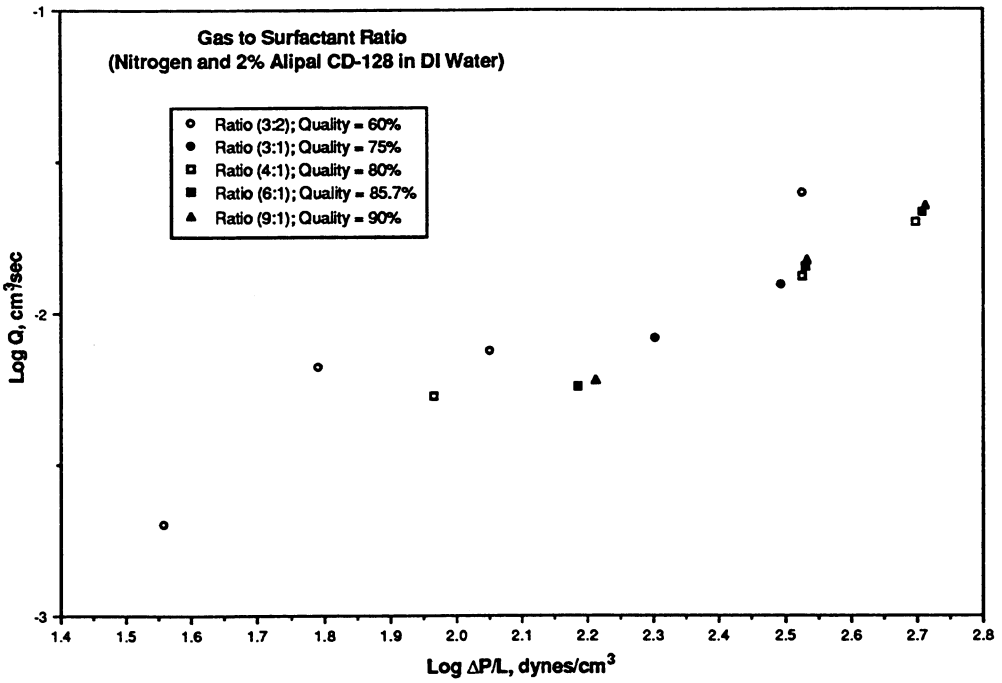

FIGURE 5. - Flow rate versus differential pressure per unit length for nitrogen + 2 wt % Alipal CD-128 in DIW at room temperature.

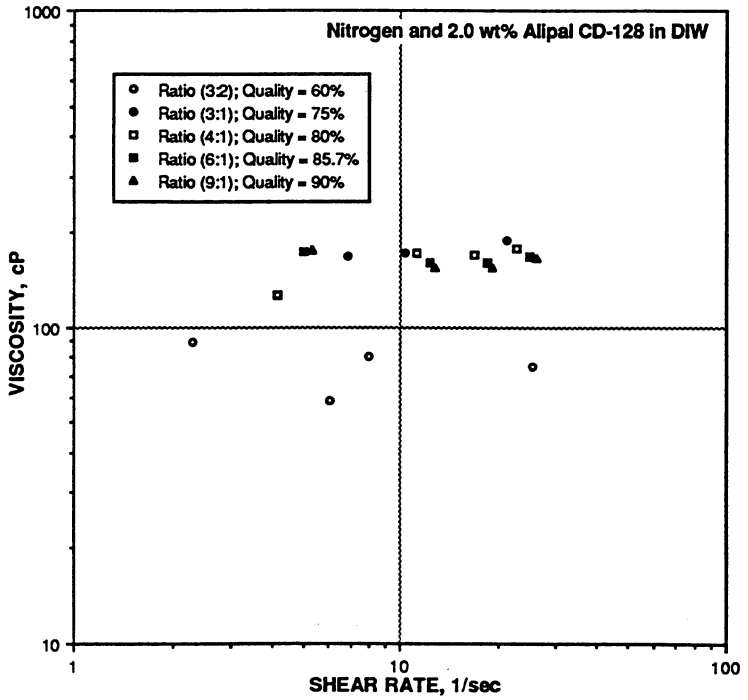

FIGURE 6. - Apparent viscosity versus shear rate for nitrogen + 2 wt % Alipal CD-128 in DIW at room temperature.

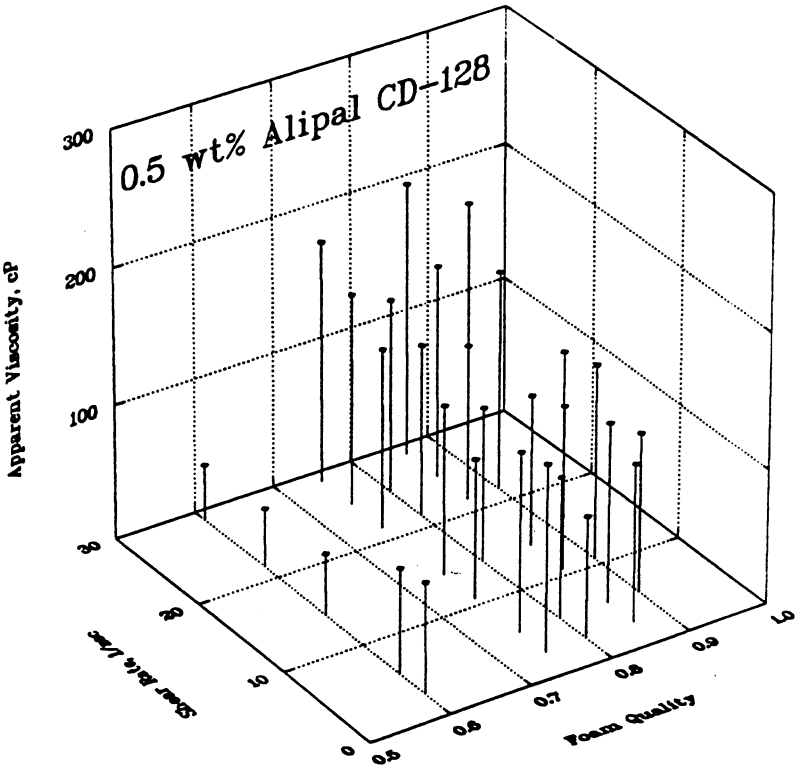

FIGURE 7. - Apparent viscosity versus shear rate and foam quality for nitrogen + 0.5 wt % Alipal CD-128 in DIW at room temperature.

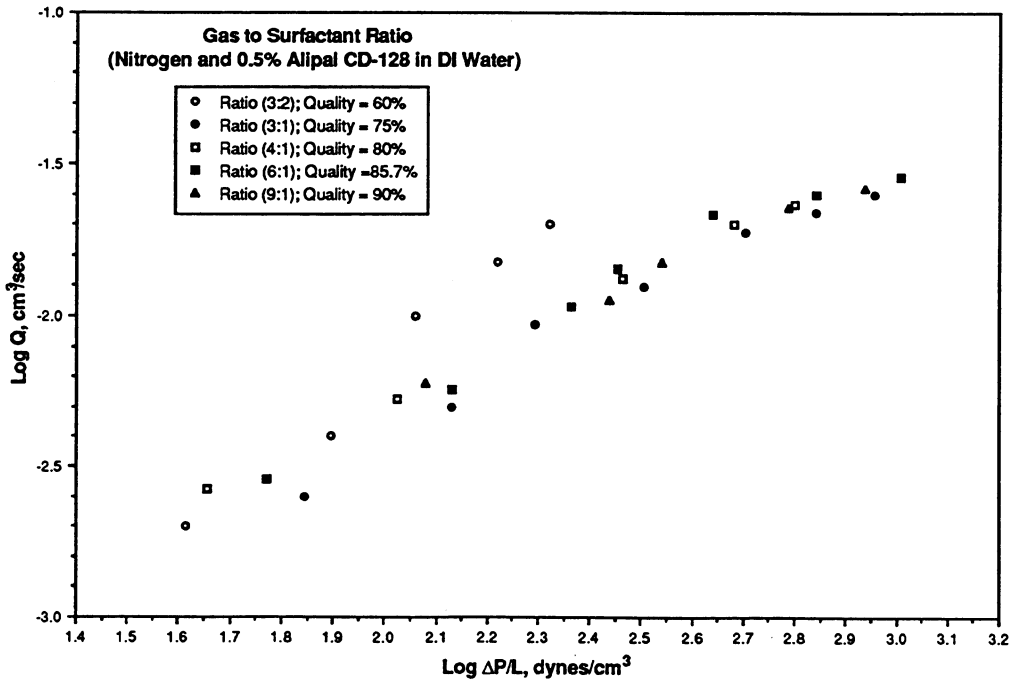

FIGURE 8. - Flow rate versus differential pressure per unit length for nitrogen + 0.5 wt % Alipal CD-128 in DIW at room temperature.

than 75%. There was no indication of the dependence of the measured apparent viscosities with the surfactant concentration. The range of viscosities measured using 0.5 and 2.0 wt % were comparable and no significant dependence was observed. Surfactant concentrations tested were above the CMC measured for this system. Economics dictate that the selection of lower surfactant concentrations would be appropriate, provided the range selected is greater than the CMC of the system under consideration. Previous studies have also shown that surfactant concentrations considerably greater than the CMC have resulted in conditions where the foam lost its stability and resiliency.[10,36]

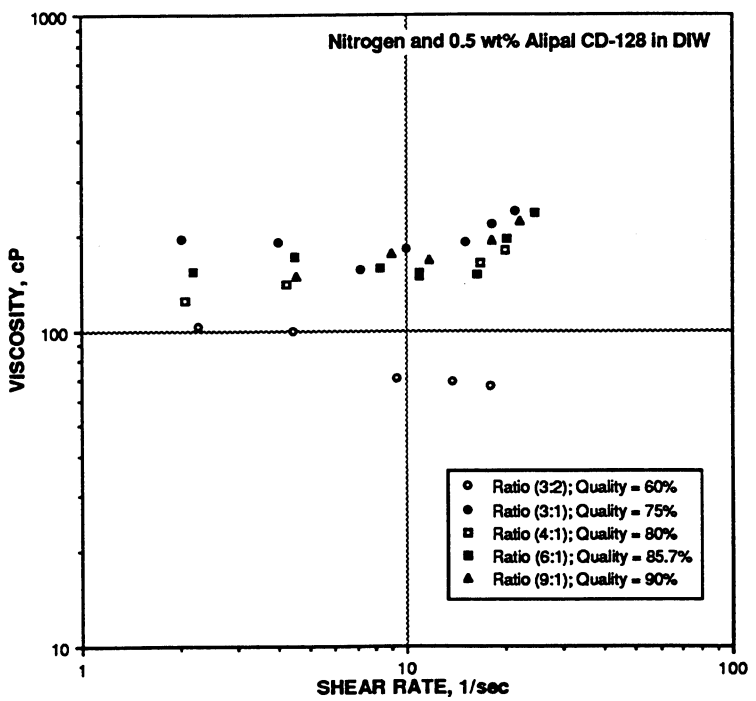

FIGURE 9. - Apparent viscosity versus shear rate for nitrogen + 0.5 wt % Alipal CD-128 in DIW at room temperature.

The temperature dependence of foam apparent viscosity was studied using a 0.5 wt % surfactant solution at 50° C. Results of the experiment are shown in figures 10 through 12. The 3-D plot of the apparent viscosity versus foam quality and shear rate is shown in figure 10. The range of viscosities measured at 50° C was comparable to, but slightly lower than the results at room temperature. The plot (fig. 11) shows the slight difference in grouping of the 60% foam data compared to qualities greater than 75%. However, unlike the experiments conducted at the lower temperature, no significant difference in trend or slope was observed. Figure 12 shows only a slight shear thinning behavior of the foam at 60% quality and a slight shear thickening behavior at qualities greater than 75%. The dependence of the measured apparent viscosities on temperature was not very significant within the range of conditions tested for this study.

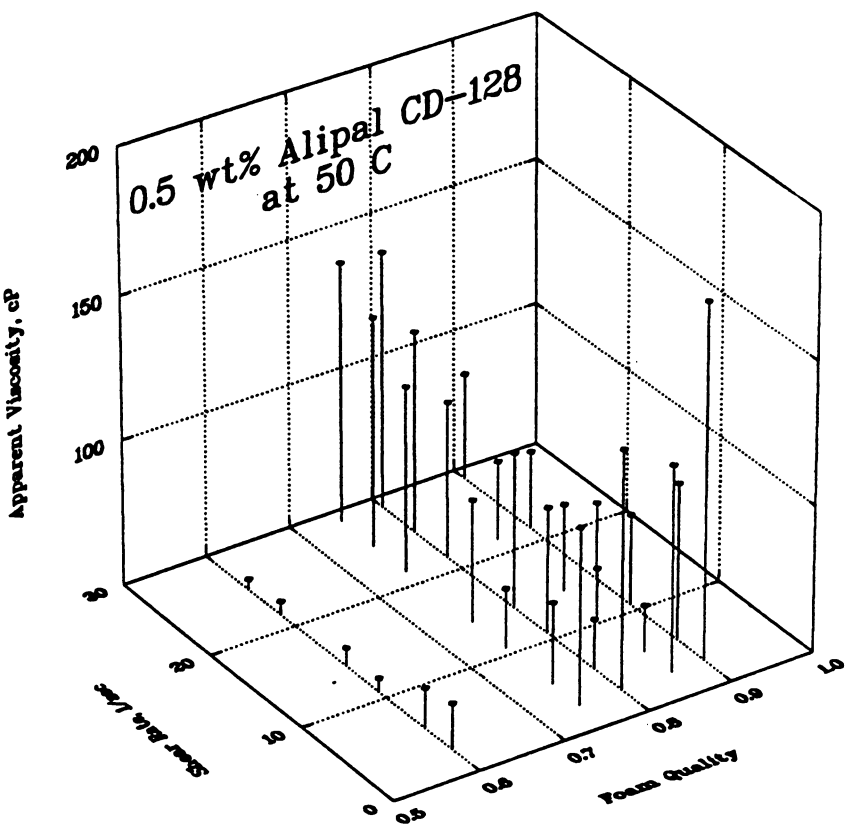

FIGURE 10. - Apparent viscosity versus shear rate and foam quality for nitrogen + 0.5 wt % Alipal CD-128 in DIW at 50° C.

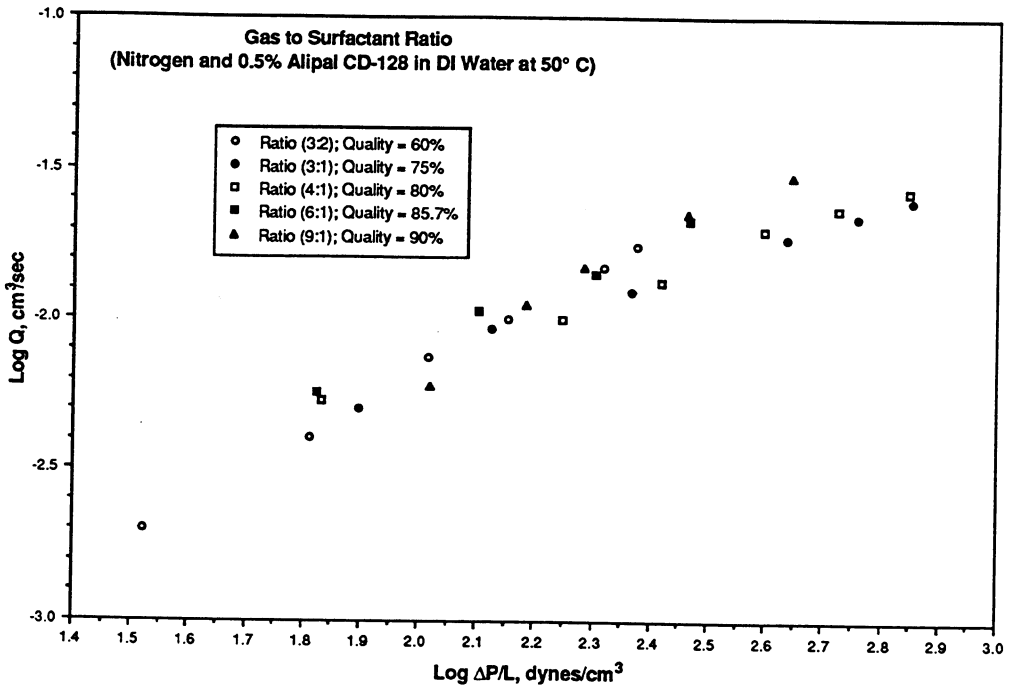

FIGURE 11. - Flow rate versus differential pressure per unit length for nitrogen + 0.5 wt % Alipal CD-128 in DIW at 50° C.

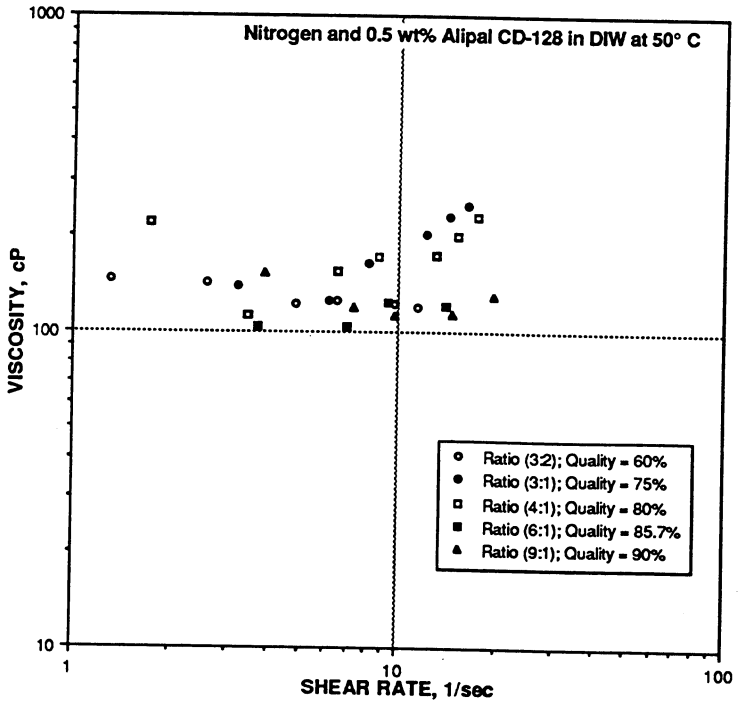

FIGURE 12. - Apparent viscosity versus shear rate for nitrogen + 0.5 wt % Alipal CD-128 in DIW at 50° C.

The bubble size distribution was determined for the experiments that were conducted. Figure 13 shows a sample comparison of the frequency distribution of the ratio of the bubble radius (r) to tube radius (R) for the different foam qualities at a range flow rates from 0.4 to 1.75 cm^3/min. The figure shows a narrow range of bubble sizes for lower foam (<90%) quality compared to a broader distribution observed for the 90% quality foam. These sample observations were made on the 0.5 wt % system at room temperature. Figure 14 shows a 3-D representation of the dependence of the bubble size ratio on foam quality and shear rate at 50° C. Bubble sizes increased with increasing quality. Bubble sizes also showed an inverse dependence on shear rate. Mean bubble sizes decreased with increasing shear rate. Figure 15 shows a comparison of mean bubble sizes at room temperature and at 50° C. There was no indication of a significant dependence of bubble sizes upon temperature. As with measured apparent viscosities, mean bubble sizes for both experiments were comparable.

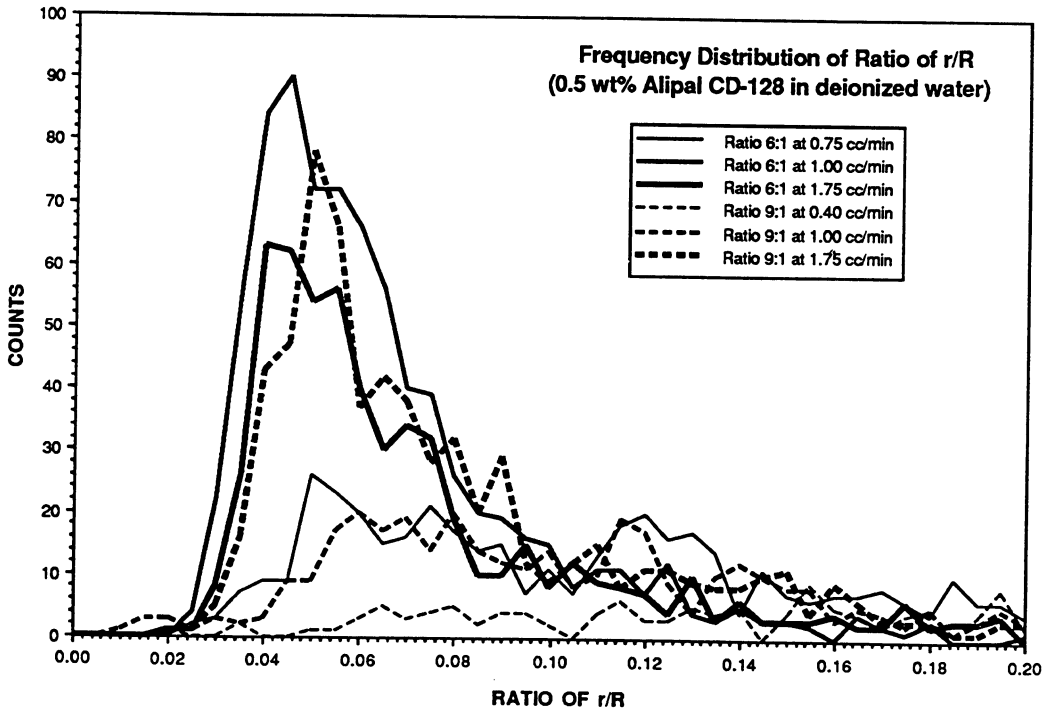

FIGURE 13. - Frequency distribution of ratio of bubble radius to tube radius for nitrogen + 0.5 wt % Alipal CD-128 in DIW at room temperature.

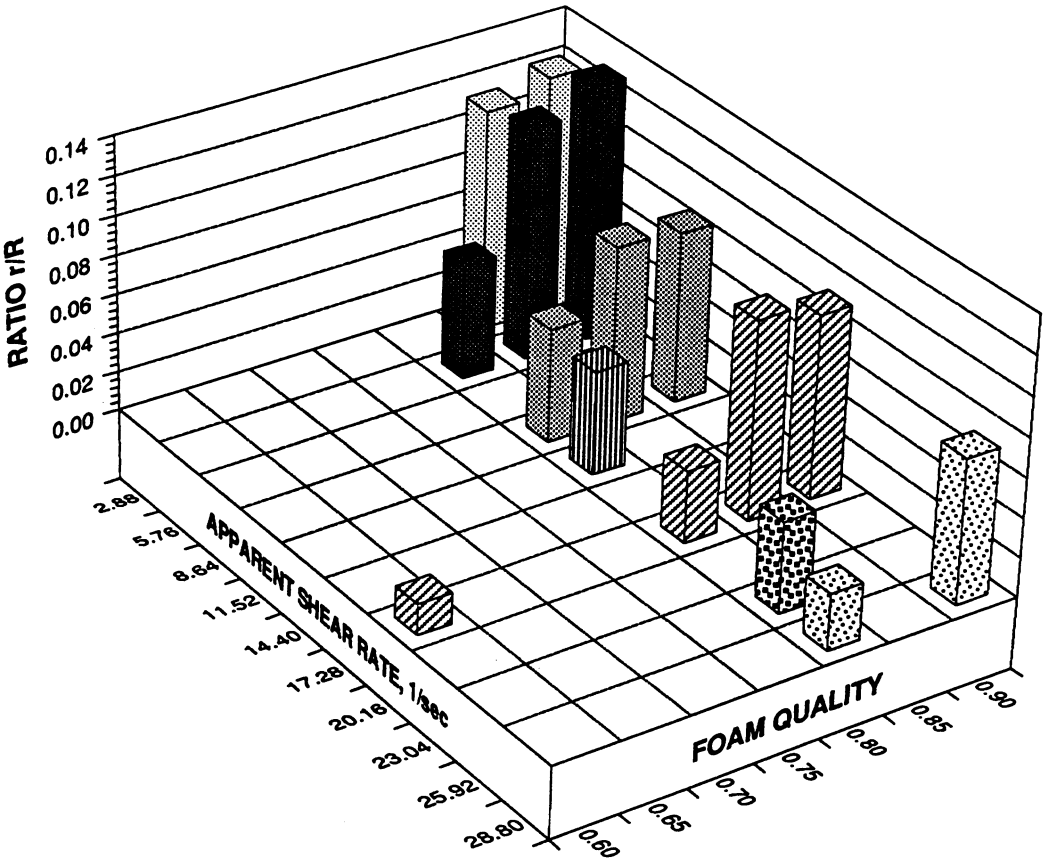

FIGURE 14. - Foam bubble size ratio versus shear rate and foam quality for nitrogen + 0.5 wt % Alipal CD-128 in DIW at 50° C.

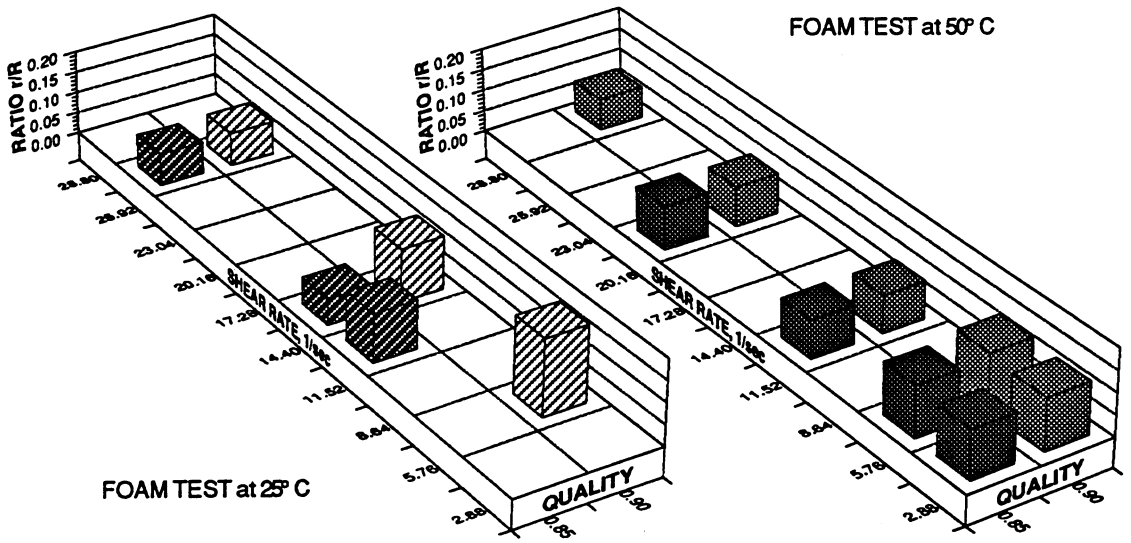

FIGURE 15. - Comparison of foam bubble size ratio versus shear rate and foam quality for nitrogen + 0.5 wt % Alipal CD-128 in DIW at room temperature and 50° C.

Overall, the results indicated that measured apparent viscosities did not significantly depend on surfactant concentrations above the CMC of the system, based on the ranges of concentrations tested. Foam viscosities only showed a slight dependence on temperature. The effects of foam quality, shear rate, and foam bubble size distribution on foam viscosity were significant. Higher foam qualities resulted in higher viscosities. The higher foam qualities also corresponded to larger bubble sizes. The dependence of viscosity on shear rate shifted from slightly shear thinning behavior at 60% quality to that of slightly shear thickening behavior above 75%. The decrease in foam bubble size also corresponded with an increase in shear rate. Results of the apparent viscosity measurements are summarized in table 2.

Foam Behavior in Packed Glass Tubes

The behavior of the flow of foam in packed glass tubes was examined. This work provided additional information on different flow regimes that may be encountered in foam applications. Apparent viscosities were measured and foam bubble size distributions were observed and recorded under different conditions. Characteristics of the homogeneous glass bead pack used in the study are listed in table 1.

Experiments were conducted with a constant backpressure of 150 psig. Variation in fluid injection ratios was accomplished by varying the flow rates of the injection pumps. The adjustment in flow rate ratios from 3:2 (gas flow rate to liquid flow rate) to 9:1 represent foam qualities (volume of gas/total volume) from 60 to 90%. The surfactant solution used for the experiments was 2.0 wt % Alipal CD-128 in deionized water. Differential pressures across the pack were determined, and the bubble size distribution in the inlet section, packed section, and outlet section of the glass tubes assembly were observed and measured.

The apparent viscosity of gas in foam under different conditions was measured. The differential pressure across the packed section was measured under conditions where pregenerated foam (using the core plug generator) was injected into the glass tube assembly. Bubble size distributions in the three sections of the assembly were measured. The differential pressure across the core was monitored until a stable differential pressure was established. Under these stable ΔP conditions, observation of foam flow behavior in the packed section showed that most of the foam bubbles in the pack were flowing uniformly. This flow behavior was previously reported under conditions called "packed-generated bubble size regime."[22]

The apparent viscosity of the gas in foam was calculated using the equation derived from Darcy's law:[22]

$$\mu_{g,\,app} = \left(\frac{Ak}{Q_g}\right)\left(\frac{\Delta P}{L}\right) \tag{8}$$

TABLE 2. - Measured apparent viscosity in the smooth capillary tube assembly

Surfactant conc., wt%	Total flow rate, cm^3/min	Foam quality, %	ΔP, psi	Apparent viscosity, cP	Comment
2.0	0.20	60.0	0.078	108.53	25° C
2.0	0.40	60.0	0.133	97.42	25° C
2.0	0.75	60.0	0.241	95.08	25° C
2.0	2.50	60.0	0.722	87.93	25° C
2.0	0.67	75.0	0.430	166.97	25° C
2.0	1.00	75.0	0.667	171.61	25° C
2.0	2.00	75.0	1.509	188.84	25° C
2.0	0.40	80.0	0.199	126.54	25° C
2.0	1.00	80.0	0.722	170.89	25° C
2.0	1.50	80.0	1.072	169.42	25° C
2.0	2.00	80.0	1.514	177.09	25° C
2.0	0.40	85.7	0.329	173.60	25° C
2.0	1.00	85.7	0.730	158.72	25° C
2.0	1.50	85.7	1.096	158.77	25° C
2.0	2.00	85.7	1.558	166.67	25° C
2.0	0.40	90.0	0.350	174.71	25° C
2.0	1.00	90.0	0.734	153.26	25° C
2.0	1.50	90.0	1.105	153.65	25° C
2.0	2.00	90.0	1.622	165.22	25° C
0.5	0.20	60.0	0.089	102.84	25° C
0.5	0.40	60.0	0.169	99.98	25° C
0.5	1.00	60.0	0.247	70.91	25° C
0.5	1.50	60.0	0.355	68.84	25° C
0.5	2.00	60.0	0.450	66.40	25° C
0.5	0.20	75.0	0.150	196.21	25° C
0.5	0.40	75.0	0.290	190.59	25° C
0.5	0.75	75.0	0.423	155.07	25° C
0.5	1.00	75.0	0.686	182.39	25° C
0.5	1.50	75.0	1.084	190.28	25° C
0.5	1.75	75.0	1.485	216.16	25° C

TABLE 2. - Measured apparent viscosity in the smooth capillary tube assembly -- continued

Surfactant conc., wt %	Total flow rate, cm^3/min	Foam quality, %	ΔP, psi	Apparent viscosity, cP	Comment
0.5	2.00	75.0	1.938	239.24	25° C
0.5	0.20	80.0	0.097	124.17	25° C
0.5	0.40	80.0	0.227	140.87	25° C
0.5	1.00	80.0	0.624	151.78	25° C
0.5	1.50	80.0	1.031	163.80	25° C
0.5	1.75	80.0	1.357	179.61	25° C
0.5	0.20	85.7	0.127	153.26	25° C
0.5	0.40	85.7	0.290	170.93	25° C
0.5	0.75	85.7	0.495	158.33	25° C
0.5	1.00	85.7	0.609	147.93	25° C
0.5	1.50	85.7	0.935	150.73	25° C
0.5	1.75	85.7	1.491	194.97	25° C
0.5	2.00	85.7	2.181	236.21	25° C
0.5	0.40	90.0	0.257	148.44	25° C
0.5	0.75	90.0	0.588	175.01	25° C
0.5	1.00	90.0	0.742	167.32	25° C
0.5	1.50	90.0	1.318	191.99	25° C
0.5	1.75	90.0	1.860	222.87	25° C
0.5	0.20	60.0	0.072	145.97	50° C
0.5	0.40	60.0	0.139	141.67	50° C
0.5	0.75	60.0	0.223	121.31	50° C
0.5	1.00	60.0	0.306	124.78	50° C
0.5	1.50	60.0	0.445	121.22	50° C
0.5	1.75	60.0	0.510	118.93	50° C
0.5	0.40	75.0	0.169	138.45	50° C
0.5	0.75	75.0	0.287	125.06	50° C
0.5	1.00	75.0	0.499	163.00	50° C
0.5	1.50	75.0	0.931	202.82	50° C
0.5	1.75	75.0	1.234	230.37	50° C
0.5	2.00	75.0	1.525	249.06	50° C

TABLE 2. - Measured apparent viscosity in the smooth capillary tube assembly -- continued

Surfactant conc., wt%	Total flow rate, cm^3/min	Foam quality, %	ΔP, psi	Apparent viscosity, cP	Comment
0.5	0.40	80.0	0.146	111.90	50° C
0.5	0.75	80.0	0.379	154.70	50° C
0.5	1.00	80.0	0.561	171.78	50° C
0.5	1.50	80.0	0.847	172.99	50° C
0.5	1.75	80.0	1.141	199.79	50° C
0.5	2.00	80.0	1.512	231.50	50° C
0.5	0.40	85.7	0.143	102.45	50° C
0.5	0.75	85.7	0.271	103.18	50° C
0.5	1.00	85.7	0.431	123.32	50° C
0.5	1.50	85.7	0.629	119.83	50° C
0.5	0.40	90.0	0.225	152.98	50° C
0.5	0.75	90.0	0.329	119.25	50° C
0.5	1.00	90.0	0.413	112.41	50° C
0.5	1.50	90.0	0.625	113.41	50° C
0.5	2.00	90.0	0.950	129.22	50° C
2.0	1.00	60.0	0.325	89.74	larger bubbles, 25° C
2.0	1.00	75.0	0.347	85.11	larger bubbles, 25° C
2.0	1.00	80.0	0.370	85.08	larger bubbles, 25° C
2.0	1.00	85.7	0.401	86.17	larger bubbles, 25° C
2.0	1.00	90.0	0.435	98.93	larger bubbles, 25° C

where $\mu_{g,\,app}$ is the apparent viscosity of the gas in cP; A is the cross-sectional area of flow in cm^2; k is the permeability in md; Q_g is the gas flow rate in cm^3/min, and ΔP is the differential pressure in psi across the length of tube, L, where it was measured. This equation was used to calculate the apparent viscosity of the gas bubble in foam of measured bubble size distribution. It was calculated in this manner for comparison with the range of viscosities observed under the conditions tested and previously reported results.[22] Results of the measurements are presented in figure 16. The plot shows a 3-D representation of the apparent viscosity as a function of the gas velocity and the foam quality (fluid-injection ratios). The plot shows the inverse dependence of the apparent viscosity of the gas with respect to an increase in gas velocity. This shows the shear-thinning behavior of this type of foam. Figure 17 shows a log-log plot of the gas viscosity versus gas velocity at different injection ratios or foam qualities. The results indicated that changes in the quality did not significantly alter the apparent viscosity in the flowing foam.

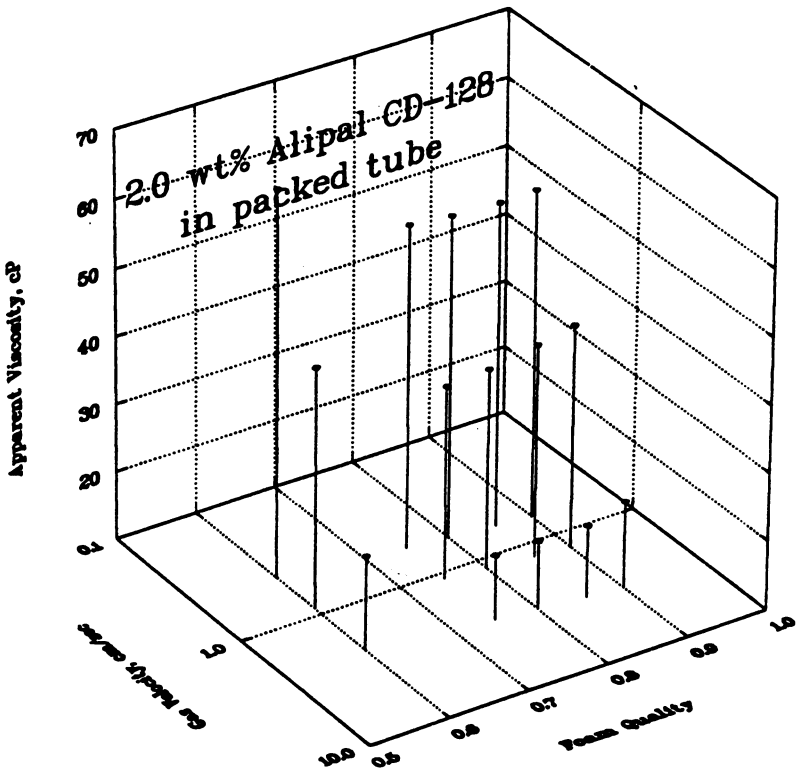

FIGURE 16. - Apparent viscosity versus gas velocity and foam quality for nitrogen + 2 wt % Alipal CD-128 in DIW at room temperature.

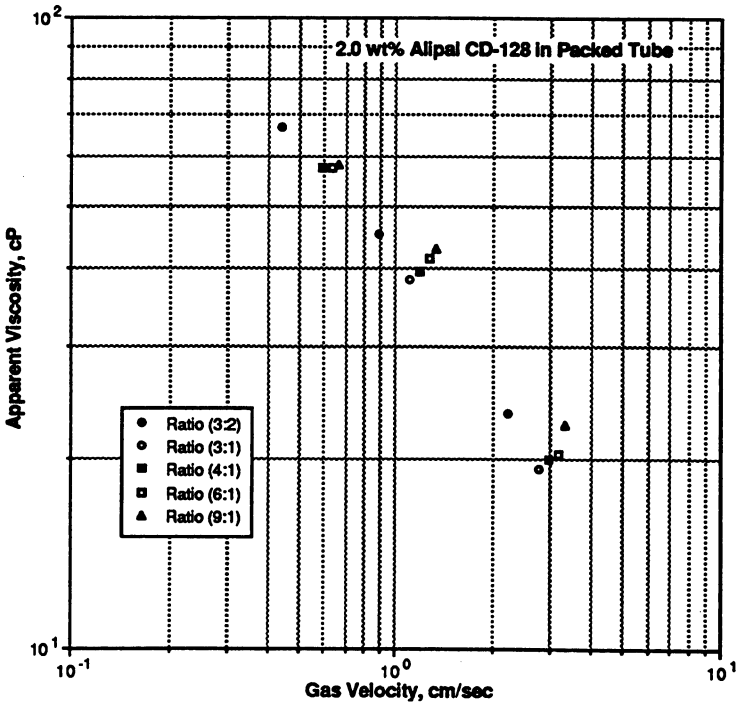

FIGURE 17. - Apparent viscosity versus gas velocity for nitrogen + 2 wt % Alipal CD-128 in DIW at room temperature.

The resistance factor across the section of packing was also determined under the different conditions tested. The resistance factor provides a measure of the effectiveness of the mobility-control agent in reducing gas mobility. This approach has been used previously in the determination of the effectiveness of polymer solutions in mobility control.[37] The resistance factor, F_R, was calculated according to the following equation:[38]

$$F_R = \frac{\left(\frac{Q}{\Delta P}\right)_{surf}}{\left(\frac{Q}{\Delta P}\right)_{foam}} \tag{9}$$

where Q is the total flow rate in cm^3/sec and ΔP is the differential pressure across the packed section in psi. Results of the experiments are shown in figure 18. This figure is a three-dimensional (3-D) plot of the resistance factor calculated as a function of total injected flow rate and foam quality (based on flow rate ratios). The plot shows that the resistance factor of the foam had some positive dependence on foam quality, at a fixed injection rate. The resistance factor increased, almost linearly, with an increase in foam quality. The effect of injection rate on resistance factors was also significant. The increase in measured resistance factors was more pronounced under low shear conditions where the total flow rate of the system was low. The relationship seemed to represent an exponential decay as a function of the increase in injection rate, indicative of shear thinning behavior. The plot indicates that at low injection rates, the foam achieved a significant decrease in mobility.

The mobility reduction can be used as a means for determining the effectiveness of foam as a mobility control agent.[14,19] The mobility reduction was calculated using an equation derived from Darcy's law:[14]

$$\lambda_R = \frac{\lambda_{foam}}{k_{surf}} = \frac{\left(\frac{Q}{A}\right)\left(\frac{L}{\Delta P}\right)}{k_{surf}} \tag{10}$$

where λ_R is the foam mobility in cP^{-1}; λ_{foam} is the foam mobility in md/cP; k_{surf} is the absolute permeability of the packed section using surfactant in md; Q is the total injection flow rate in cm^3/min; A is the cross-sectional area of flow in cm^2, ΔP is the differential pressure in psi across the length of tube, L, over which it was measured. The term λ_R accounts for the reduced ratio of the mobility of the foam with respect to that of the surfactant. The results are presented in figure 19. The plot shows the mobility reduction as a function of the gas velocity for the different flow rate ratios tested. The reduced mobility ranged from as low as 0.02 to as high as 0.07 cP^{-1}, within the injection rates tested. As a mobility-control agent the foam's mobility reduction corresponded to effective viscosities ranging from 14 to 50 cP.

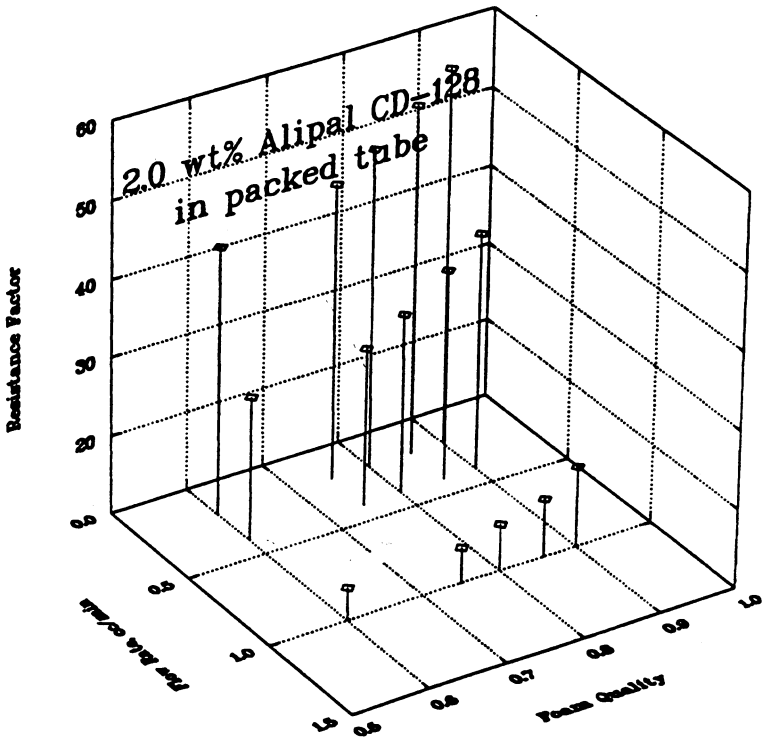

FIGURE 18. - Resistance factor versus total flow rate and foam quality for nitrogen + 2 wt % Alipal CD-128 in DIW at room temperature.

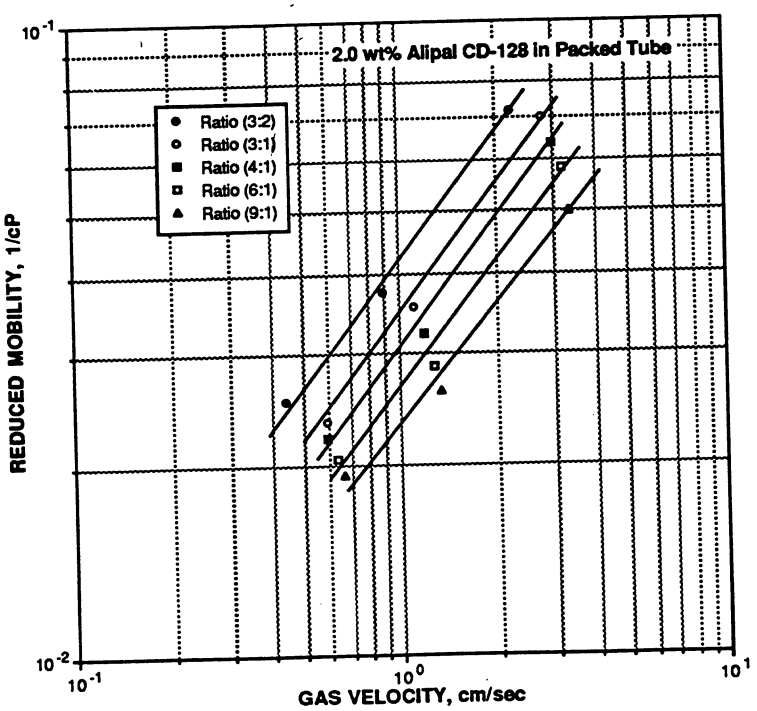

FIGURE 19. - Mobility reduction versus gas velocity for nitrogen + 2 wt % Alipal CD-128 in DIW at room temperature.

Foam bubble size distributions under different conditions were observed and recorded in the three sections of the glass assembly. The results are presented in figures 20 through 25. Figures 20 through 22 show the ratio of the bubble size to glass tube radius (r/R) at the different foam qualities (injection ratios), under different total injection rates (shear rates). These figures show bubble size ratios for the inlet section, packed section, and outlet section of the glass tube assembly, respectively. The results indicate that the larger bubbles sizes were apparent at high foam quality conditions in the inlet and outlet sections of the assembly. The bubble size distribution in the packed section seemed to be more uniform as is shown in figure 21. This uniformity of the bubble size distribution in the packed section could account for the absence of the effect of the foam quality on the measured gas apparent viscosity, as was shown in figures 16 and 17. Figures 23 through 25 show a comparison of the ratio of the bubble radius to glass tube radius as a function of the foam quality, at each of the injection rates tested. The results showed that the ratio of bubble sizes followed the order of:

$$r/R_{\text{inlet section}} \geq r/R_{\text{outlet section}} \gg r/R_{\text{packed section}}.$$

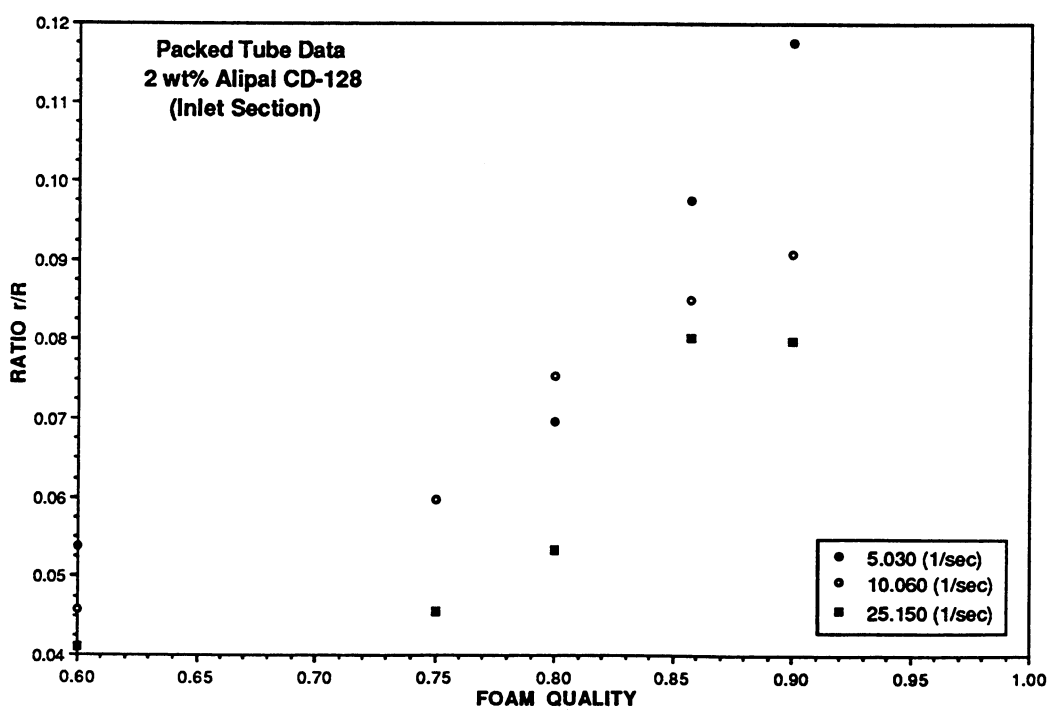

FIGURE 20. - Foam bubble size ratio versus foam quality in the inlet section of the packed tube assembly.

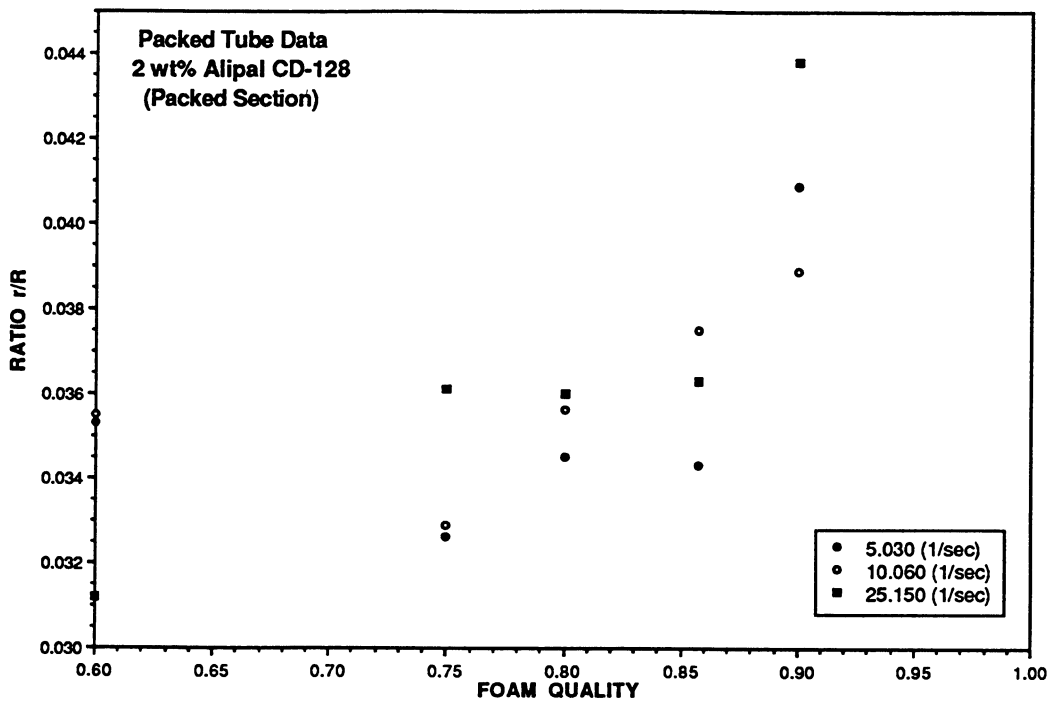

FIGURE 21. - Foam bubble size ratio versus foam quality in the packed section of the packed tube assembly.

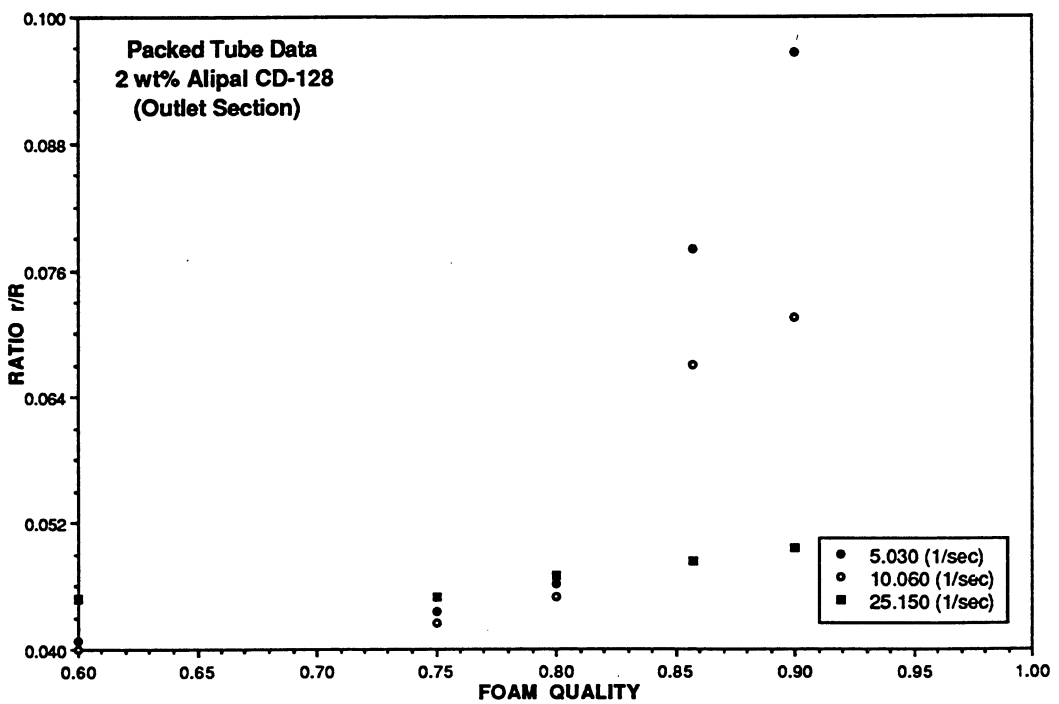

FIGURE 22. - Foam bubble size ratio versus foam quality in the outlet section of the packed tube assembly.

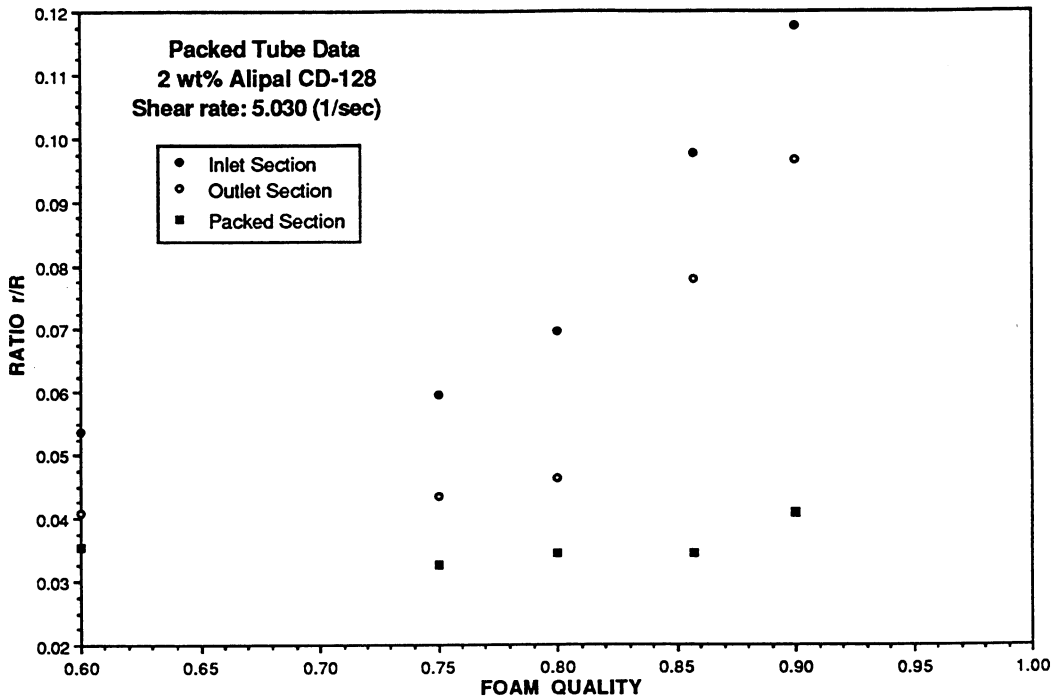

FIGURE 23. - Foam bubble size ratio versus foam quality in the inlet section of the packed tube assembly at a shear rate of 5.03 sec^{-1}.

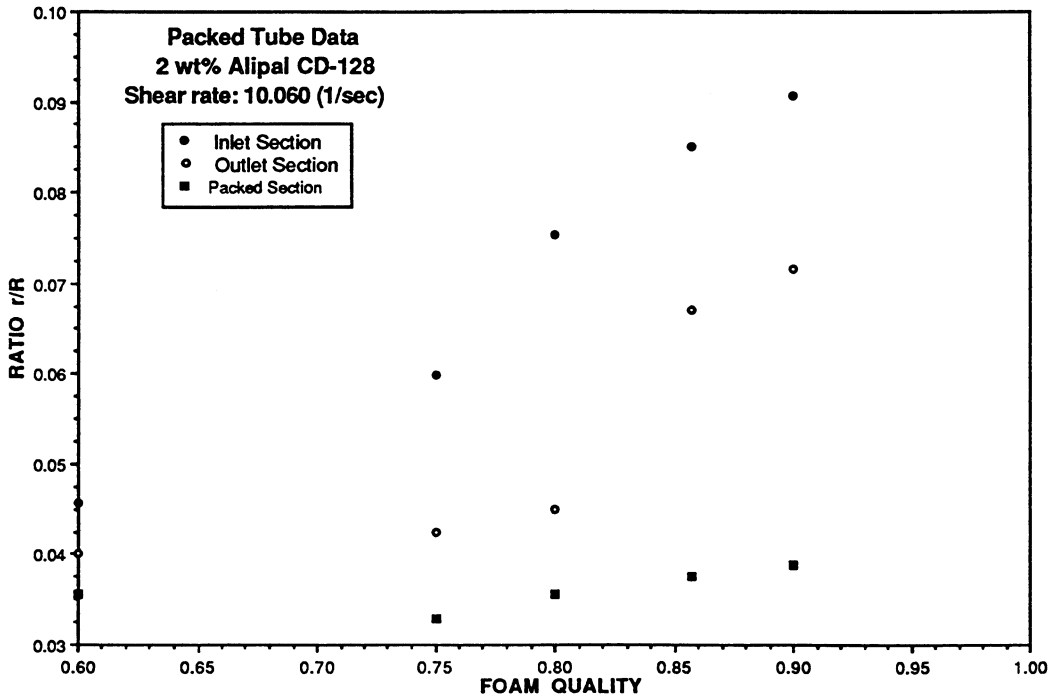

FIGURE 24. - Foam bubble size ratio versus foam quality in the inlet section of the packed tube assembly at a shear rate of 10.06 sec^{-1}.

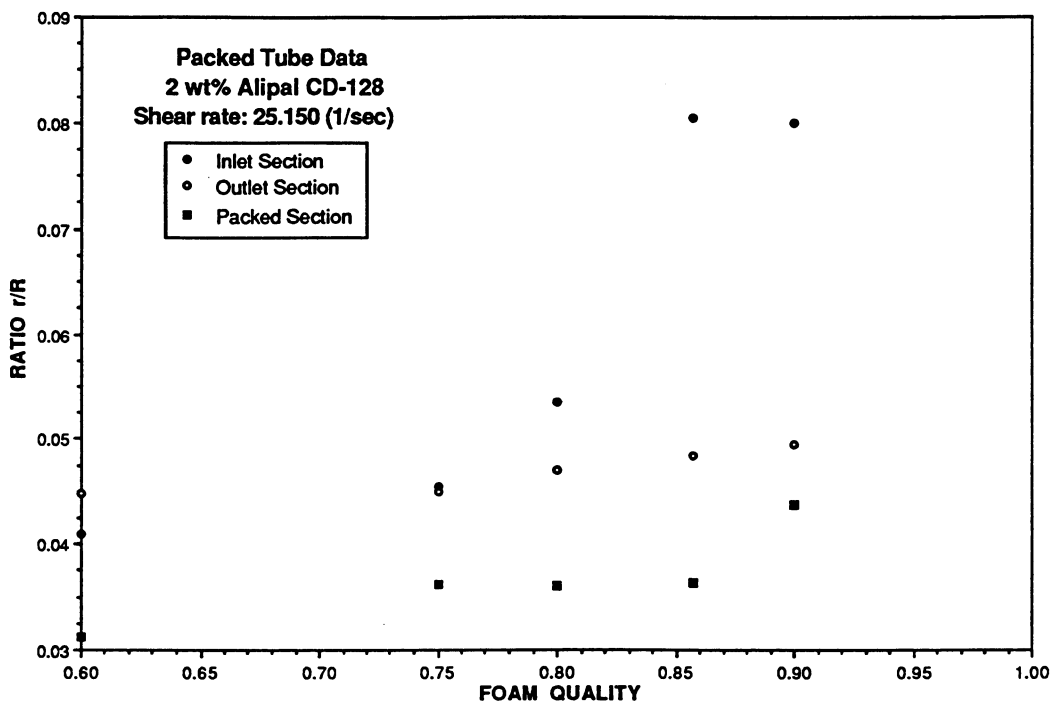

FIGURE 25. - Foam bubble size ratio versus foam quality in the inlet section of the packed tube assembly at a shear rate of 25.15 sec^{-1}.

Bubble size distributions in the inlet and outlet section were comparable, whereas bubble sizes in the packed section were smaller but fairly uniform in distribution considering the variation in foam quality and injection rates tested. Results of the viscosity measurements are summarized in table 3.

Comparison Calculations Using Predictive Model for Foam Apparent Viscosity

A mathematical model for the prediction of the apparent viscosity of foam flowing through smooth capillaries was developed by Hirasaki and Lawson.[21] Their approach was based on developing a conceptual model of natural porous media as a representation of a bundle of interconnected capillaries of different sizes with constrictions. The component of foam flow and resistance to flow under conditions in smooth, uniform pore sections was approximated by flow and resistance in smooth and uniform capillaries. They pointed out that the most important variable affecting foam viscosity in smooth capillaries was foam texture (bubble size). Foam of finer texture has more lamellae per unit length, and as a result, greater

TABLE 3. - Measured apparent viscosity in the packed glass tube assembly

Foam quality, %	Total flow rate, cm^3/min	ΔP, psi	Resistance factor	Reduced mobility, cP^{-1}	Gas velocity, cm/sec	Apparent viscosity, cP
90.0	1.00	62.411	20.30	0.0500	3.33	22.59
85.7	1.00	53.647	17.45	0.0582	3.17	20.39
80.0	1.00	48.951	15.92	0.0638	2.96	19.93
75.0	1.00	44.518	14.48	0.0701	2.77	19.34
60.0	1.00	43.480	14.14	0.0718	2.22	23.61
90.0	0.40	47.448	40.38	0.0263	1.33	42.93
85.7	0.40	43.484	37.01	0.0287	1.27	41.31
80.0	0.40	38.717	32.95	0.0323	1.18	39.41
75.0	0.40	35.308	30.05	0.0354	1.11	38.34
60.0	0.40	33.348	28.38	0.0375	0.89	45.26
90.0	0.20	32.282	58.17	0.0193	0.67	58.42
85.7	0.20	30.432	54.83	0.0205	0.63	57.83
80.0	0.20	28.260	50.92	0.0221	0.59	57.54
75.0	0.20	26.579	47.89	0.0235	0.55	57.72
60.0	0.20	24.616	44.35	0.0254	0.44	66.82
surfactant only	1.00	3.075	–	–	–	–
surfactant only	0.40	1.175	–	–	–	–
surfactant only	0.20	0.555	–	–	–	–

[1]Surfactant concentration - 2.0 wt %.

resistance to flow. Their findings stipulate three factors that can affect the apparent viscosity of foam in uniform capillaries related to the dynamic changes at the gas/liquid interfaces: (1) the effect of the slugs of liquid between gas bubbles on flow resistance; (2) the effect of viscous and capillary forces on the extent of the deformation of interfaces and resulting bubble shapes; and (3) the effect of the formation of surface tension gradients along the bubble interfaces attributed to the expansion and compression of the bubble during flow. The model they developed accounts for these three factors as described by the equation:

$$\mu_{app} = \mu^{shape} + \mu^{liquid} + \mu^{gradient} \tag{11}$$

where μ^{shape} is the contribution of the deformation of interfaces and resulting bubble shape on apparent viscosity, described as:

$$\mu^{shape} = 0.85\left(\frac{\mu n_L R}{r_c / R}\right)(3\mu U/\sigma)^{-1/3}[(r_c/R)^2 + 1] \tag{12}$$

The μ^{liquid} is the contribution of the slugs of liquid between bubbles to resistance to flow, described as:

$$\mu^{liquid} = \mu L_s n_L \tag{13}$$

The $\mu^{gradient}$ is the contribution of the presence of the surface tension gradient at the bubble interface to the apparent viscosity, described as:

$$\mu^{gradient} = (\mu n_L R)(3\mu U/\sigma)^{-1/3}\sqrt{N_s}\left(\frac{1 - e^{-N_L}}{1 + e^{-N_L}}\right) \tag{14}$$

In equations 12 through 14, μ is the liquid viscosity in cP; R is the tube radius in cm; n_L is the number of lamellae per unit length of tube; U is the flow velocity in cm/sec; r_c is the radius of curvature of the gas/liquid interface in cm; σ is the surface tension of the surfactant solution in dynes/cm; L_s is the length of liquid slugs between bubbles in cm and parameters N_s and N_L are dimensionless variables describing the surface tension effect and length of thin film portion of the bubble, respectively. A description of the theoretical basis for the development of the model has been described in Reference 21.

Results of these experiments were compared to the prediction using the mathematical model. Appropriate experimental variables were used to account for the difference in conditions encountered in the two studies. Experimental parameters used in the calculations are listed in table 4. Aside from these variables, the values of parameters β and $2/(P)_c$ were assumed to be similar to ones determined in the paper [21] (β = 5 cm.; $2/(P)_c$ = 1.0). This assumption could account for some degree of error in the prediction. These parameters were assumed to be constant since they were only used in the evaluation of the contribution of the surface tension gradient. The results of the mathematical predictions are shown in figure 26. The plot shows the effect of changing the foam quality on the apparent viscosity and a comparison of the predicted apparent viscosity with that of the experimental data. The data points reported in the paper were plotted against the prediction of that set of data points.[21] A clear indication of agreement between the experimental data points from the paper and prediction can be seen. Deviation occurred at the region where the foam quality was greater than 90%. The model was also used to predict the apparent viscosity based on our experimental conditions. The values of the predicted viscosities and our experimental results did not agree for the two sets of experiments that were conducted, under the conditions noted on the graph. In both cases, the mathematical model resulted in an over-prediction of the apparent viscosity of the foam by as much as a factor of 10. The difference in experimental conditions between the prior work[21] and this experimental study could be one factor that contributed to the lack of agreement. Bubble sizes in the present study were considerably smaller than (i.e., 4 to 6 times smaller)

TABLE 4. - Experimental parameters used in the predictive model calculations

Inside diameter, cm	0.228
Length, cm	148.0
Packing material	glass beads
Average bead diameter, cm	0.035
Ratio of r_B/R_{cap}	1.38
R_{cap}, cm	[1]0.0056
Permeability (k), D	105.6
Surface tension, dynes/cm	32.0
Liquid viscosity, cP	0.95
β, cm	5
$(P)_c$	2

[1]Calculated from equation 16.

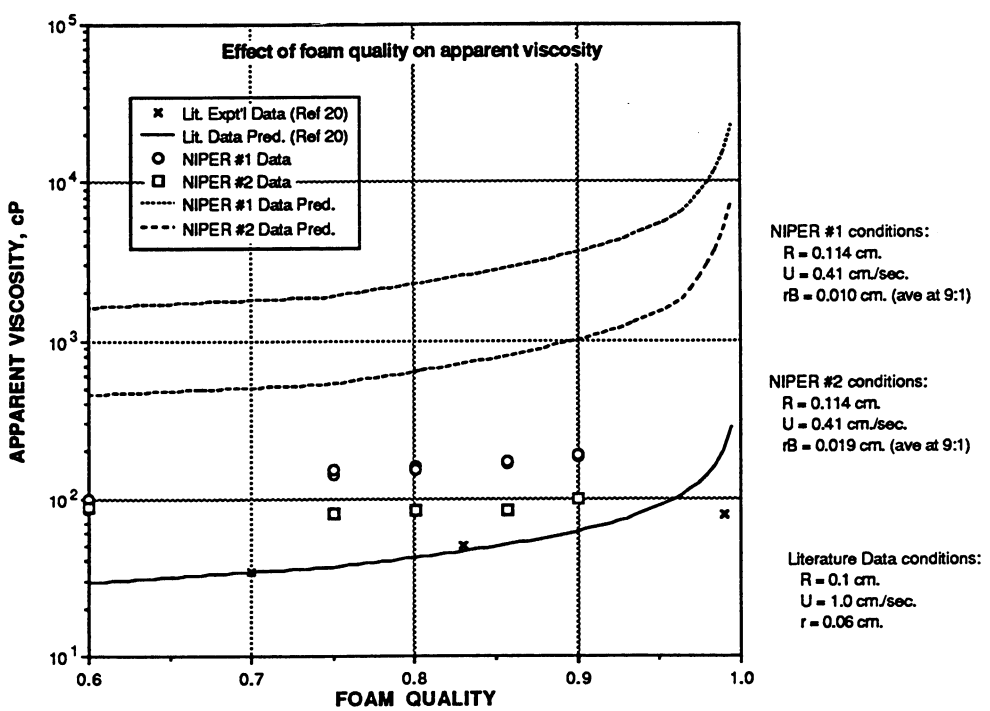

FIGURE 26. - Comparison of predicted and measured apparent viscosity versus foam quality in smooth capillary tubes.

than results reported by Hirasaki and Lawson.[21] Figure 27 shows a comparison of the range of viscosity values for the two sets of experiments conducted. The experiments were conducted in a slightly different manner to generate different bubble size distributions. The plot in figure 27 shows the values of apparent viscosities measured.

The dependence of the prediction of the apparent viscosity on the ratio of the bubble radius to tube radius (r_B/R) is very significant. Figure 28 shows a plot of the apparent viscosity as a function of the ratio of the bubble to the tube radius, (r_B/R). The conditions of the two sets of experiments were not quite similar but the present study showed that the model predicted greater apparent viscosities of the foam than was observed. The predicted range of viscosities were about an order of magnitude higher than experimentally measured. Judging from the trend of the prediction, as the ratio of r_B/R becomes infinitely small, the apparent viscosity becomes increasingly larger. This trend may not be correct since as the r_B/R becomes infinitely small, the apparent viscosity should gradually decrease to the value of the surfactant viscosity. This dependence on r_B/R, at very small values of the apparent viscosity has to be properly accounted for by the model. The measured bubble size ratio may not be of practical application under reservoir condition, but the results do show that there is significant difference in predicted values under the size regimes considered. Extrapolation to condition where r_B/R becomes infinitely small may not be realistic and the model fails to account for this boundary condition.

The flow of foam in smooth capillaries is one component of the flow of foam through porous media. The work of Hirasaki and Lawson[21] was extended to account for the conditions where the pore constrictions contributed to the behavior of the flow of foam. The extension by Falls et al[22] considers the apparent viscosity of gas in foam to be contributed by two components, expressed as:

$$\mu_{app} = \mu^{smooth} + \mu^{constriction} \tag{15}$$

where μ^{smooth} comes from the theory developed from foam flow in smooth capillaries,[21] while $\mu^{constriction}$ represents the contribution to the viscosity term based on effect of pore constrictions. The application of the model for the viscosity of foam in smooth capillary was similar except in cases where the tube radius was expressed as an equivalent capillary radius equal to:[33]

$$r_{cap} \equiv 2r_H \equiv \frac{\phi\, d_b}{\left(3[1-\phi] + \frac{2d_b}{d_t}\right)} \tag{16}$$

where r_H is the hydraulic radius of the pack, ϕ is the porosity, d_b is the bead diameter and d_t is the tube diameter.

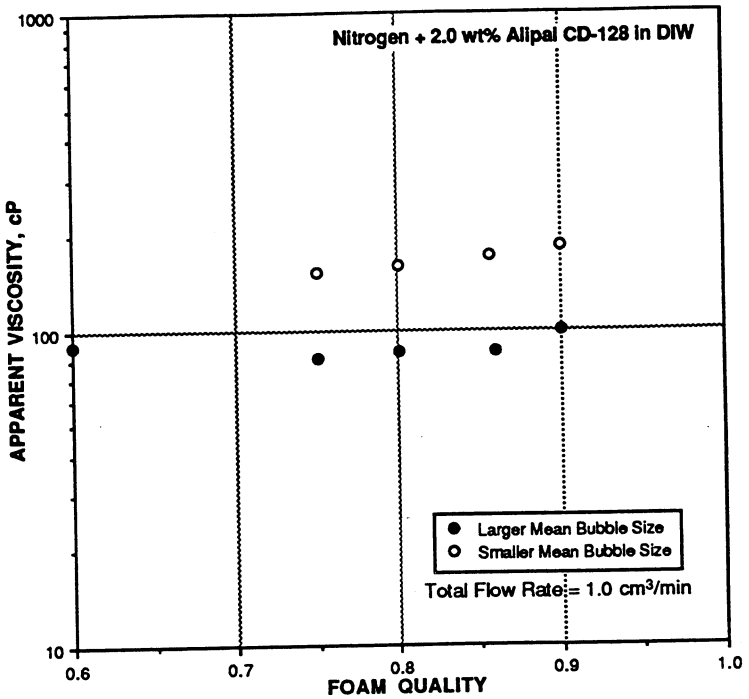

FIGURE 27. - Comparison of measured apparent viscosity versus foam quality for nitrogen + 2 wt % Alipal CD-128.

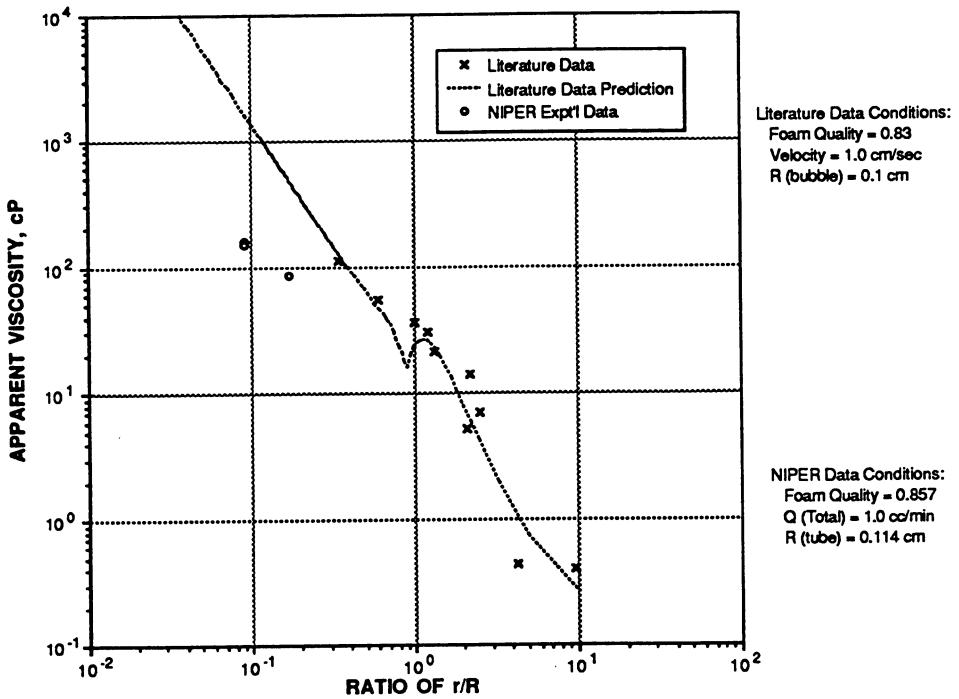

FIGURE 28. - Comparison of predicted and measured apparent viscosity versus ratio of r_B/R in smooth capillary tubes.

The general expression for the viscosity term due to constrictions, $\mu^{constriction}$ is expressed as:

$$\mu^{cons} = (\xi_1 \mu n_L r_{cap}) (3\mu U / \sigma)^{-1} \qquad \text{for } n_L \ll n_{pc} \qquad (17)$$

$$\mu^{cons} = \xi_2 (3\mu U / \sigma)^{-1} \qquad \text{for } n_L \gg n_{pc} \qquad (18)$$

where μ is the viscosity of the surfactant solution in cP, U is the gas bubble velocity in cm/sec, σ is the surface tension of the surfactant solution in dynes/cm, n_L is the number of lamellae per unit length, n_{pc} is the number of constrictions per unit length, and ξ_1 and ξ_2 are experimentally determined parameters to account for the contribution of pore constrictions to the apparent viscosity. Reference 22 presents the development of this extended model.

The extended mathematical model and the smooth capillary model were used to compare the results of the experiments conducted in the packed glass tube assembly. Results of the comparison are presented in figure 29. It shows a plot of the measured apparent gas viscosity as a function of the gas

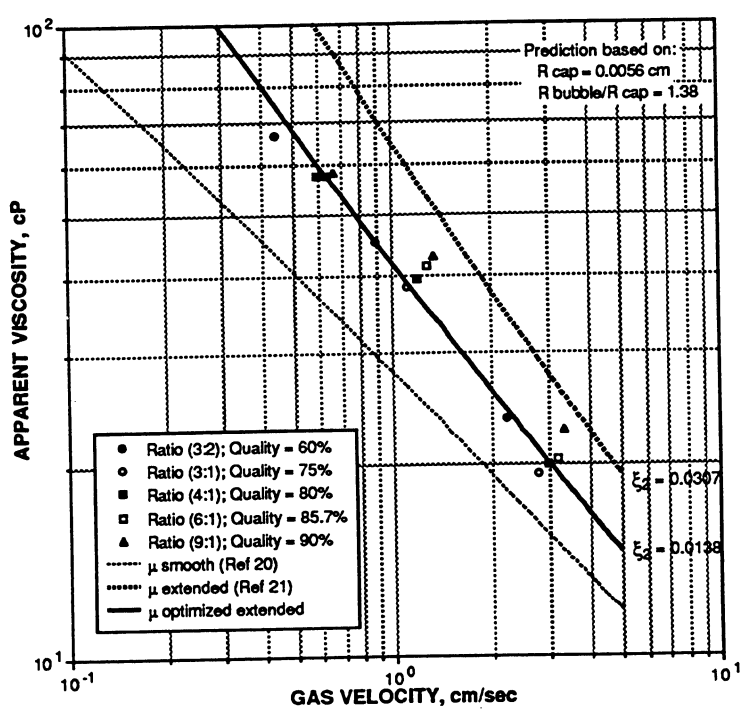

FIGURE 29. - Comparison of predicted and measured apparent viscosity versus gas velocity in packed glass tubes.

bubble velocity compared with the predicted values using the smooth capillary model and the extended model. The plot shows that the smooth capillary model predicted low values of apparent viscosity of the gas in the foam within the gas velocity range tested. This was consistent with what was previously reported in the literature.[22] The predicted values indicated that the contribution of the flow of foam in smooth capillaries was only one of the components of the flow through bead packs and the contribution of the complexity of the pore constrictions on the apparent viscosity has to be included. A critical assumption that has been made in the calculations was that the capillary pressure behavior in the bead packs was similar. The capillary pressure function derived for hexagonal packing of uniform spheres was used.[22] This function was used in determining the radius of curvature of plateau borders in a foam lamellae, r_c. The value of r_c had a direct effect on the calculated viscosity terms from equations 12 and 14. The model developed for apparent viscosity in smooth capillary tubes did not over predict the values of the apparent viscosities in the packed tube, unlike the case with the measurements using the smooth capillary tubes. This could be attributed to the difference in the ratio of r_B/r_{cap} (1.38) and r_B/R (0.09) for the two sets of experiments. The ratio of the radii in the packed tube were considerably larger than the ones in the smooth capillary tube. The model developed for smooth capillaries did not correctly predict the cases when the ratio of the radius was less than 0.1.

The extended model was applied using equation 18. The selection of this equation was based on the visual and recorded observations of the foam flow in the packed section of the glass tube assembly, where $n_L > n_{pc}$ (number of lamellae per unit length > number of constrictions per unit length). Using the extended model to account for the effect of the pore constrictions, the model predicted slightly greater values of apparent viscosities over the range of conditions studied. One reason for this over prediction was the value of the parameter ξ_2 (0.037)[21] used in the calculations. This parameter serves as a weighting function to account for the contribution from pore constrictions. The ξ_2 parameter has to be evaluated from the measurements conducted in this study to properly predict the range of measured apparent viscosities. The same value (0.037) of the parameter[21] was used in the calculation in order to provide an indication of the degree of viscosity correction that was incorporated. Figure 29 also shows the agreement of the traces of the predicted apparent viscosities with the measured values using the optimized ξ_2 parameter of 0.0138. The ξ_2 parameter was therefore optimized to obtain a better fit.

EFFECT OF INJECTION RATE ON FOAM PERFORMANCE

Foam flow systems involve multiphase flow, which includes gas, water, surfactant solution, and oil phases. Multiphase flow in porous media is controlled by many factors such as the wettability of the medium, pore structure, fluid distributions, and fluid properties. Experiments were conducted to determine the effect of injection rate on foam generation. Coreflood experiments were conducted in the presence of gas, water, and surfactant solution only, without any oil present. Nitrogen gas was injected to

displace brine or surfactant solution at different injection rates. These coreflood experiments were conducted in a relatively homogeneous Berea sandstone core (1.5-in. diameter and 5-in. long) at 75° F and 1,500 psig. The surfactant solution used was a 1 wt % Alipal CD-128 in 5 wt % NaCl solution, and the brine used was a solution of 5 wt % NaCl in deionized water.

The first coreflood test involved nitrogen displacing brine. Nitrogen gas was continuously injected into a brine saturated core to displace the brine. Results of this test are shown in figure 30. The ultimate brine recovery was 45%, and the gas breakthrough was at about 0.45 PV injection. The total pressure drop across the 5-in.-long core was about 2 psi, at an injection rate of 50 cm^3/hr. When the nitrogen injection rate was lowered to 5 cm^3/hr, the brine recovery was slightly lower (38%), and gas broke through a little earlier. The second coreflood test involved nitrogen displacing the surfactant solution at a low injection rate of 5 cm^3/hr. The injection process was the same as that of the first experiment. As shown in figure 31, the recovery of surfactant solution was much greater than that of brine. However, there was no significant increase in pressure gradient or delay in gas breakthrough during the experiment. Visual observation from the sight glass at the outlet end of the core indicated that no foam was generated during the gas flood. The third coreflood test was similar to the second experiment except for the higher injection rate of 50 cm^3/hr. Results of this experiment are shown in figure 32. There were significant differences in the time for gas breakthrough and pressure drop in this experiment compared to the results of the second coreflood. In the third experiment, the pressure gradient across the core responded immediately after gas injection and increased to 60 psi. The pressure gradient remained constant even after gas breakthrough. The gas breakthrough was also significantly delayed. Fine bubbles were observed in the outlet sight glass during the flooding. These results show that gas flow rate is an important factor for effective foam generation. Under reservoir conditions, the velocity of the injected gas is high near wellbores, but decreases sharply with the radial distance. Foam generation at wellbores would not present a substantial problem, but it may be difficult to generate foam at downstream locations, partly because of the dilution of surfactant concentration.

The situation becomes more complicated in formations containing oil. The three phases: oil, gas, and brine may flow separately in the pore paths. As illustrated in figure 33, if foam is generated to block a gas channel in a tertiary recovery mode, the injected surfactant solution must fill the gas channel. The injected surfactant solution tends to flow where the brine phase went, instead of into gas-occupied space. In this case, the injected surfactant solution will not be fully utilized for foam generation. The gas will still channel through, unless the amount of the injected surfactant solution is large enough to fill the gas channel. This situation is illustrated in figure 33-3A, and is believed to be one of the major factors that contribute to the failure of field tests. If the surfactant solution is injected at a high rate, it may be able to fill all gas paths near the wellbore. In this case, foam can be generated near the injection well and may

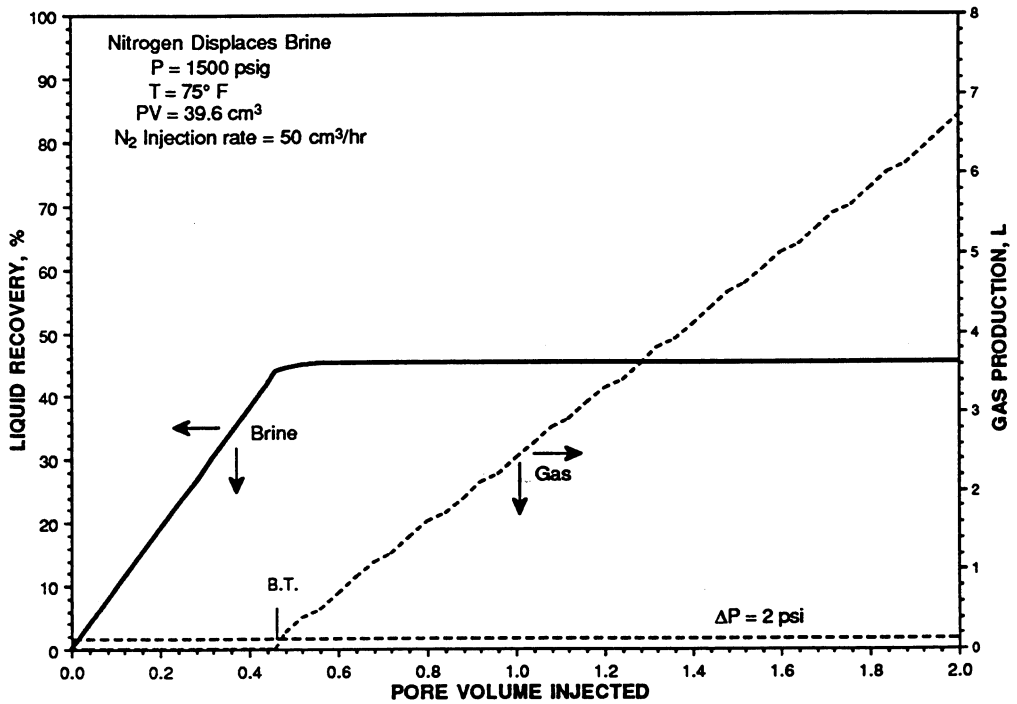

FIGURE 30. - Coreflood no. 1: Nitrogen displacing brine at 50 cm^3/hr.

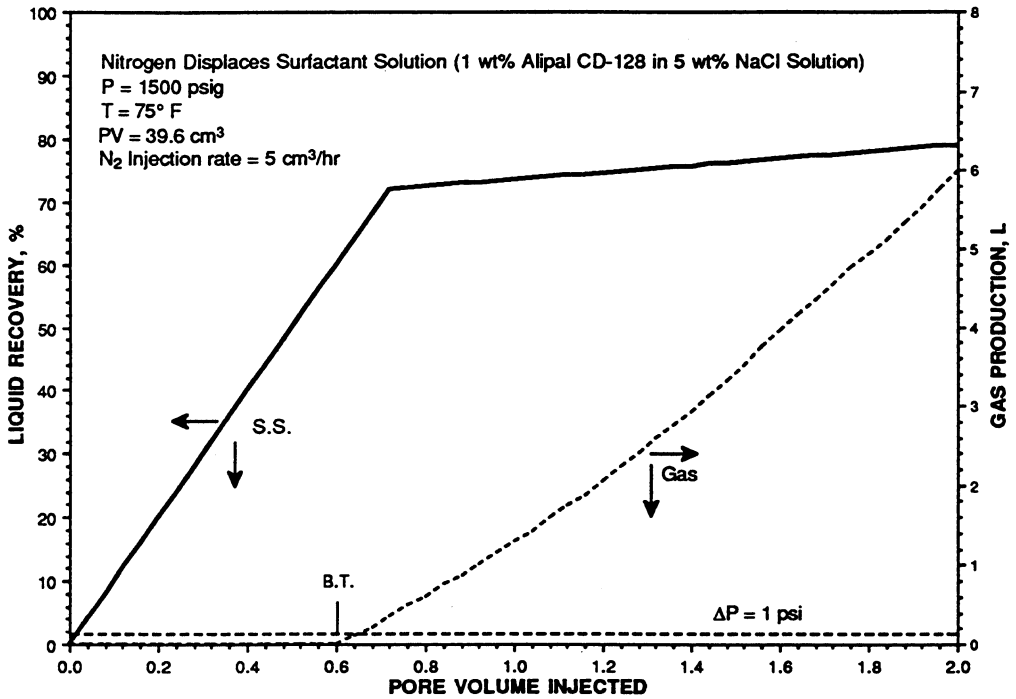

FIGURE 31. - Coreflood no. 2: Nitrogen displacing surfactant solution at 5 cm^3/hr.

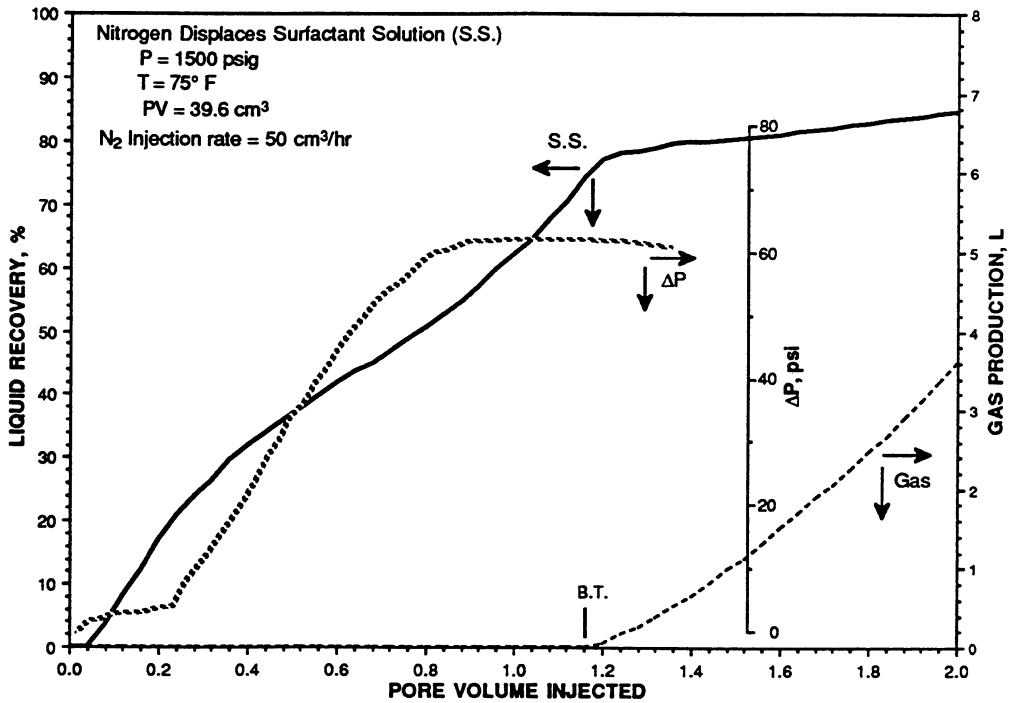

FIGURE 32. - Coreflood no. 3: Nitrogen displacing surfactant solution at 50 cm^3/hr.

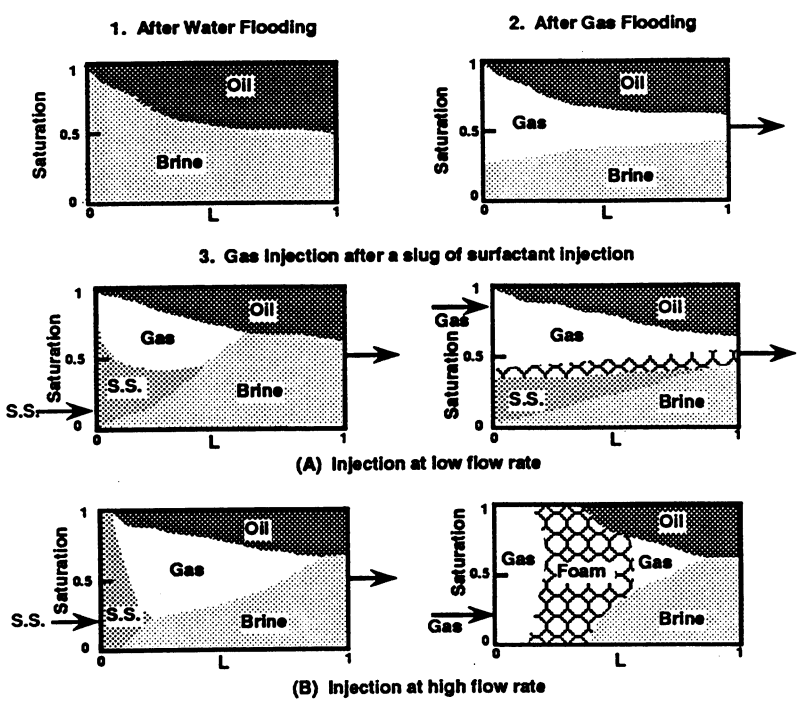

FIGURE 33. - Effect of injection rate on foam generation.
(* s.s. = surfactant solution)

propagate to a certain distance from the injection well, as illustrated in figure 33-3B. In field applications, how to control and route the injected surfactant solution to fill the gas channel becomes an essential design factor for the success of foam technology. Formation heterogeneity and surfactant adsorption complicate the foam performance even more, making its behavior even more difficult to control and predict.

EFFECT OF FOAM ON GAS SWEEP IMPROVEMENT AND GAS-WATER RELATIVE PERMEABILITY

The Effectiveness of Foam for Gas Sweep Improvement

Dual-core foam floods were conducted to study the diversion of gas flow from a high-permeability zone to a low-permeability zone. Using two cores connected together in parallel, fluids were allowed to flow preferentially through a high-permeability core, just as injected fluids do through high-permeability zones in a flooded oil reservoir. Foams, whether injected as foam or formed in situ by gas fingering through a liquid foaming solution, can redirect flow to the lower-permeability zones which are usually not flooded. The foam was formed in situ in these experiments

Experimental Apparatus and Procedure

A series of experiments was designed as constant-pressure tests, using a nitrogen gas blanket common to all the fluid vessels to displace the fluids into the cores at low injection pressures (5.0 psig ±0.01 psi). The outlet pressure was atmospheric. Figure 34 is a schematic diagram of the experimental apparatus. Two unfired Berea sandstone cores were connected together in parallel, simulating different reservoir zones. They were cast in epoxy and had significantly different permeabilities. All cores were cylindrical, 1.5 -in.-diameter. They were first cleaned with brine, isopropanol, and methanol (in that order), then dried with nitrogen and evacuated before each test. Each core was then fully saturated with 5.0 wt % NaCl brine, and the brine was injected long enough to establish the beginning permeability of each core. The three test fluids used were the 5.0 wt % NaCl brine, a foamer consisting of 1.0 wt % active Alipal CD-128 surfactant in the same brine, and nitrogen gas. The four experiments consisted of different injection sequences of those fluids, changing fluids without stopping flow by means of a four-way selector valve.

Experimental Results and Discussion

The first test used cores A (87 md, 12.0 in. long) and B (395 md, 12.0 in. long) mounted vertically. The initially brine-saturated cores were flooded with nitrogen gas, injected from the top, to residual water saturation. Figure 35 shows the much higher mobility of gas through core B. A 0.1-PV (pore volume) slug of foamer was then injected, followed by continuous nitrogen. As figure 35 shows, the mobility of gas through high-permeability core B was reduced to near zero. Gas mobility in core A decreased, but not as much. Obviously, most of the foaming solution entered core B, as expected, but a minute amount also

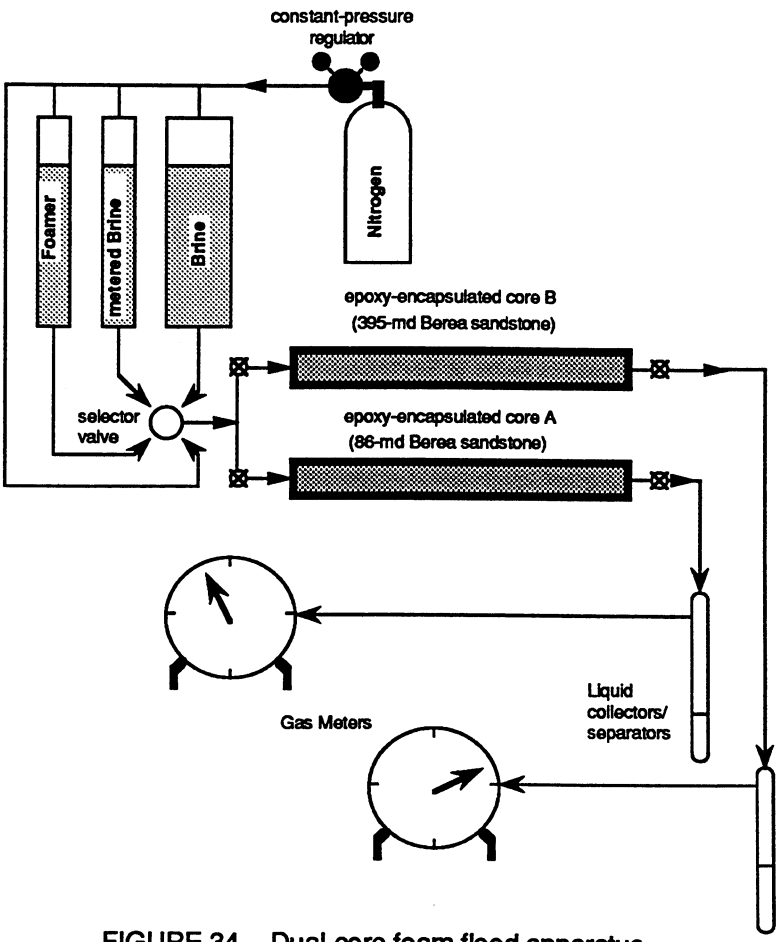

FIGURE 34. - Dual-core foam flood apparatus.

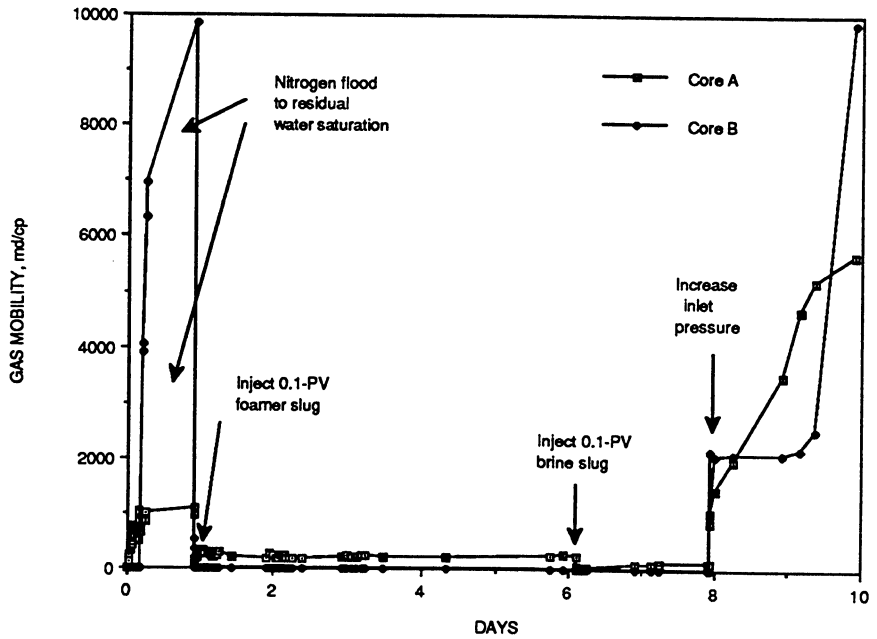

FIGURE 35. - Gas mobility history of dual-core foam flood #1: cores vertical.

entered A, also as expected. A foam was formed in each. After several days of constant nitrogen flow through core A, a 0.1-PV slug of brine was injected in an attempt to dilute the foam blocking B and restricting flow in A. Most or all of the brine entered core A , as evidenced by the reduced mobility through that core. No change was seen in core B. After about half of a day, the mobility of gas in core A levelled at a value somewhat less than before brine injection. Then, the test pressure of 5 psig was increased to 20 psig to test the strength of the foams. Gas flow through both cores, and therefore mobility, increased immediately and continued to increase until the test's end. The foam was not able to withstand the higher pressure gradient of 20 psi/ft. It quickly collapsed, and nitrogen mobility increased as the foaming solution was displaced from both cores.

For the second test, the same two cores were set horizontally. The brine-saturated cores were flooded with nitrogen gas to residual water saturation. A 0.1-PV slug of foamer was then injected, followed by continuous nitrogen. As figure 36 shows, the mobility of gas through the higher-permeability core B was reduced to approximately one one-thousandth of the pre-foam level. Gas mobility in core A decreased to approximately one-third of its previous level. Obviously, most of the foamer entered core B, but a minute amount also entered A, as expected. A foam was formed in each, effecting the desired diversion of flow. The cores were X-ray scanned by computed tomography (CT-scanned) upon being filled with brine, then at residual water saturation, and again at the conclusion of the foam flood. Comparisons of these different density images, representing slices along the cores, were intended to help interpret the movement of fluids through the floods, but interpretation of the images was difficult. Density contrasts due to different fluids were smeared due to inadequate resolution of the scanner.

The third coreflood used cores C (85 md, 11.13-in. long) and D (549 md, 11.25 in. long) in a horizontal position, so that gas would finger through the liquid. After testing the very temporary reduction in gas mobility by injection of two separate 0.1-PV brine slugs (the WAG process), a 0.1-PV foamer slug was injected. This resulted in the desired diversion of flow from D to C, shown in figure 37. The fourth dual-core foam flood was a baseline experiment, using only brine and gas without surfactant, to help interpret behavior of the previous experiments. Cores C and D were oriented vertically. Its gas mobility history is shown in figure 38. It is a much smoother curve than the wildly varying plots for foamer slug tests.

Flow in these foam experiments did not reach equilibrium. Flow rates were always varying, never settling to any smooth curve. Use of small slugs of foamer may result in such unpredictable behavior.

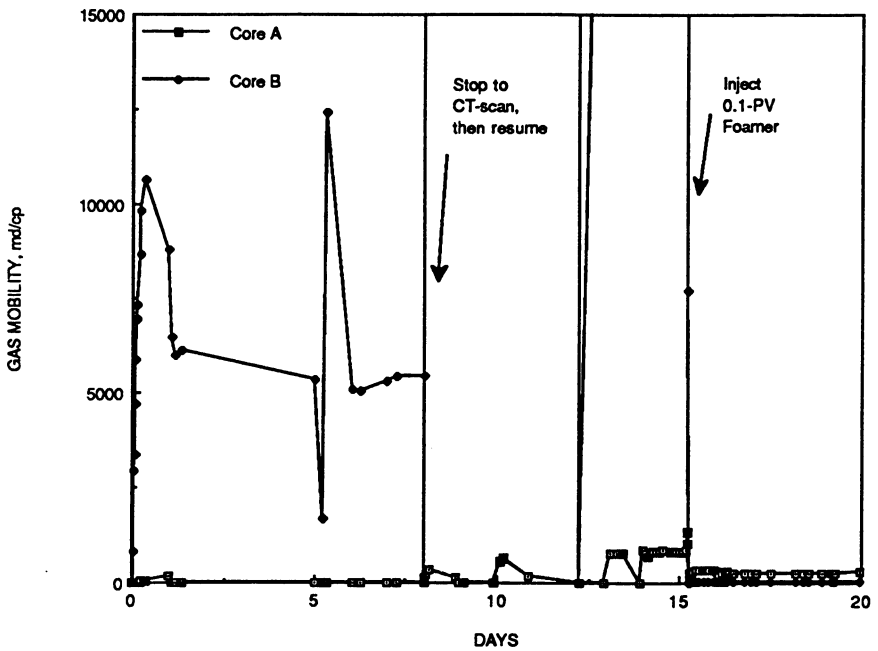

FIGURE 36. - Gas mobility history of dual-core foam flood #2: cores horizontal.

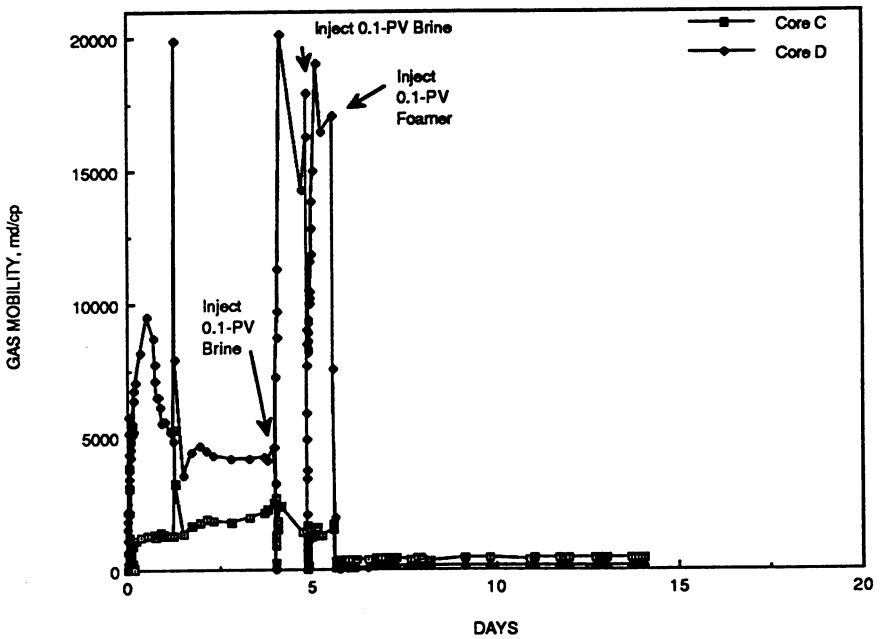

FIGURE 37. - Gas mobility history of dual-core foam flood #3: cores horizontal.

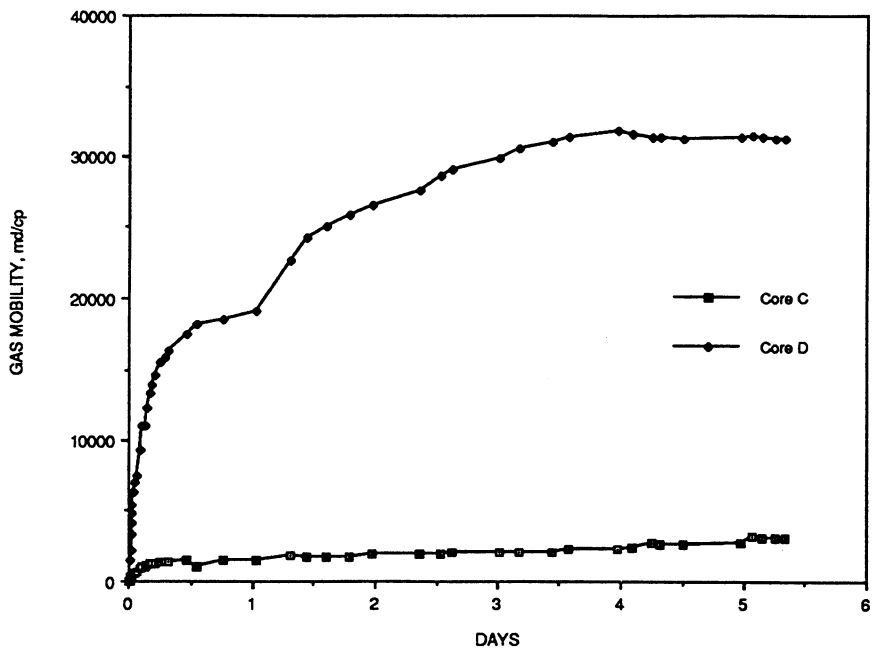

FIGURE 38. - Gas mobility history of dual-core foam flood #4: cores vertical.

Effect of Foam on Gas-Water Relative Permeabilities

For reservoir numerical simulation, some of the most useful, and usually necessary, information is a set of relative permeability curves. These curves show how different fluids interact with each other to affect their flow through a reservoir. To simulate the use of foam for sweep improvement in gas flooding, a simulator would need relative permeability curves including foam. To simplify the highly complex behavior of foam, in this study foam was not considered as a separate moving entity, but rather, the effect of the foaming solution (surfactant solution) upon the gas-water relative permeabilities was considered. Gas-water relative permeabilities were measured wherein the water was a foaming solution in one experiment and merely brine in another identical experiment. Huh and Handy[39] used the same philosophy of treating the foaming solution as the water phase in their study to determine the difference between steady-state and unsteady-state experiments.

Experimental Apparatus and Procedure

Relative permeability experiments used the same constant-pressure coreflooding apparatus used in the dual-core gas sweep improvement experiments discussed previously. The layout is the same as that shown in figure 34, except that only a single core was used. Each core used was a fired 1.5-in.-diameter cylindrical Berea sandstone. They were similarly solvent-cleaned, dried, and evacuated between

tests. Fluids differed from the dual-core study in their concentrations -- the brine contained 0.5 wt % NaCl, and the foamer consisted of 0.5 wt % active Alipal CD-128 in that brine. All floods were conducted with the cores in the horizontal position. Inlet pressures were either 2.5 or 5.0 psig, and outlet pressures were atmospheric. To begin each test, the evacuated core was fully saturated with either brine or foamer, then this liquid was allowed to flow through long enough to establish an initial permeability to water. Without stopping flow, the injection was switched to nitrogen gas to conduct an unsteady-state displacement. From the produced liquid and gas volumes versus time data, gas-water relative permeabilities were calculated using the Jones and Rozelle[40] method, which is the graphical equivalent to the classical Johnson-Bossler-Naumann method.[41] It is especially useful for constant-pressure experiments such as those conducted in this work. All relative permeabilities calculated were referenced to the initial liquid permeability for each test, such that the liquid relative permeabilities were equal to unity at 100% liquid saturation.

Six experiments are described in table 5, and their results are listed in table 6. The first core used was 4.92 in. long and was mounted in a rubber sleeve coreholder. Its water permeability was first determined to be 132 md. The first test was a baseline experiment which consisted of injecting nitrogen gas into the brine-saturated core at a constant 2.5 psig until residual water saturation. The second test was similar to the first, except that the same core was initially saturated with foamer before injecting nitrogen. The third was a repeat of the first to confirm results. Therefore, only the results of the third test, instead of the first, will be reported and discussed.

TABLE 5. - Experimental parameters for gas-liquid relative permeability measurements

Test	Initial saturating liquid	Core length, in.	psi	psid/ft	Core permeability, md	Core	Porosity
No. 2	foamer	4.9	2.5	6.1	132	E	0.244
No. 3	brine	4.9	2.5	6.1	323	E	0.240
No. 4	foamer	12.0	2.5	2.5	560	H	0.236
No. 5	foamer	12.0	5.0	5.0	557	H	0.238
No. 6	brine	12.0	5.0	5.0	1,246	H	0.237
No. 7	brine	12.0	2.5	2.5	1,263	H	0.237

All were constant-pressure experiments conducted in fired Berea sandstone cores (1.5 in. diameter).

TABLE 6. - Results of relative permeability measurements

Test	Gas Breakthrough Time, min.	Frontal Velocity ft/D[1]	Shear rate, sec^{-1}	Average water saturation at gas breakthrough	Residual water saturation	Final gas rel. permeability	Final foam M.R.F.[2]
No. 2	23.0	25.67	215	0.474	0.307	0.0166	0.102
No. 3	10.0	59.04	211	0.761	0.559	0.1623	—
No. 4	66.0	21.82	92	0.419	0.238	0.0131	0.025
No. 5	17.5	82.29	331	0.473	0.161	0.0239	0.028
No. 6	2.3	617.14	1,042	0.792	0.256	0.8592	—
No. 7	6.0	240.00	387	0.808	0.334	0.5159	—

[1]Calculated from start of gas injection until gas breakthrough.

[2]M.R.F. = Mobility reduction factor = $\frac{\text{Final gas relative permeability with foamer}}{\text{Final gas relative permeability with brine}}$ at same conditions.

The remaining tests, 4 through 7, used a 12-in.-long cores encapsulated in epoxy. Test 4 used a 12.0-in.-long core initially saturated with foamer, into which was injected nitrogen at 2.5 psig. Test 5 was the same, except that the inlet pressure was 5.0 psig. Tests 6 and 7 used the same core initially saturated with brine, at inlet pressures of 5.0 and 2.5 psig, respectively.

Experimental Results and Discussion

The calculated gas-water relative permeability data are plotted in figures 39 through 44. Since the gas displaced the wetting liquid, these are drainage curves which move from right to left on the plots of relative permeability versus water saturation. The foaming solution had a significant effect upon the shape and magnitude of the relative permeabilities curves. The foaming solution, with its lower interfacial tension, decreased the residual water saturation from the brine-only tests in every case: from 0.56 to 0.31 in low-permeability core E at 6.1 psi/ft (tests 3 and 2, figs. 40 and 39, respectively), from 0.33 to 0.24 in high-permeability core H at 2.5 psi/ft (tests 7 and 4, figs. 44 and 41, respectively), and from 0.26 to 0.16 in core H at 5.0 psi/ft (tests 6 and 5, figs. 43 and 42, respectively). It thereby also resulted in lower average water saturation at gas breakthrough. The foamer delayed gas breakthrough and decreased the frontal

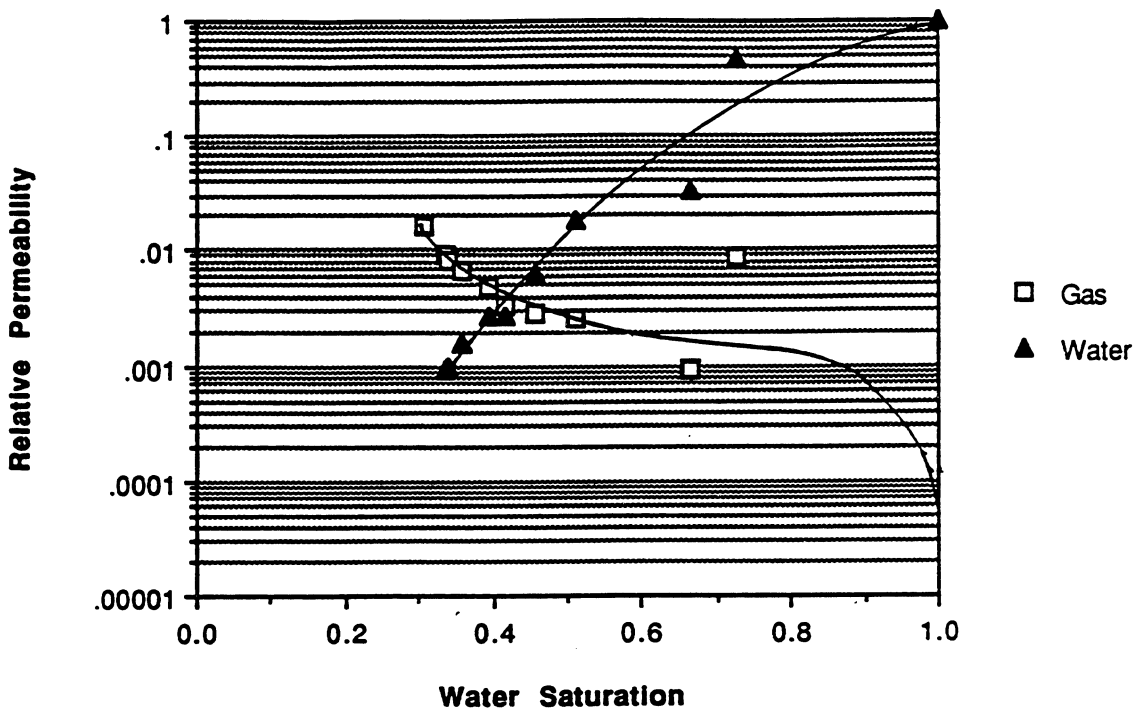

FIGURE 39. - Gas-water relative permeability test no. 2, using foamer at 6.1 psi/ft in a low-permeability core.

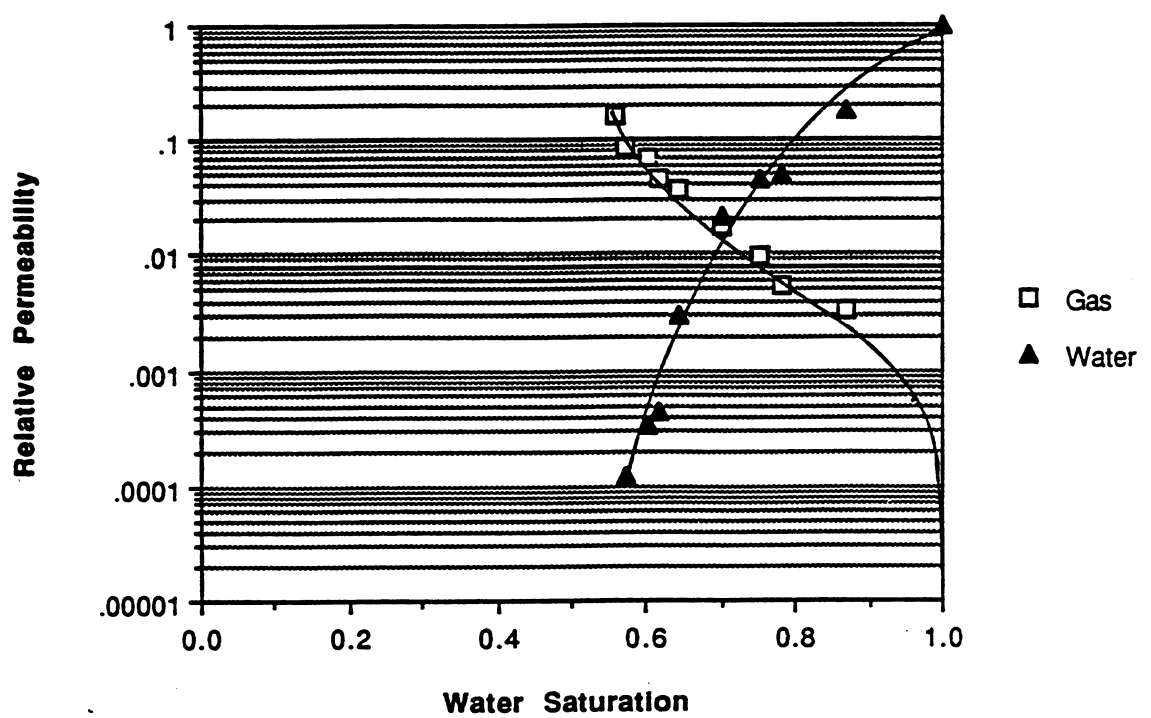

FIGURE 40. - Gas-water relative permeability test no. 3, using brine at 6.1 psi/ft in a low-permeability core.

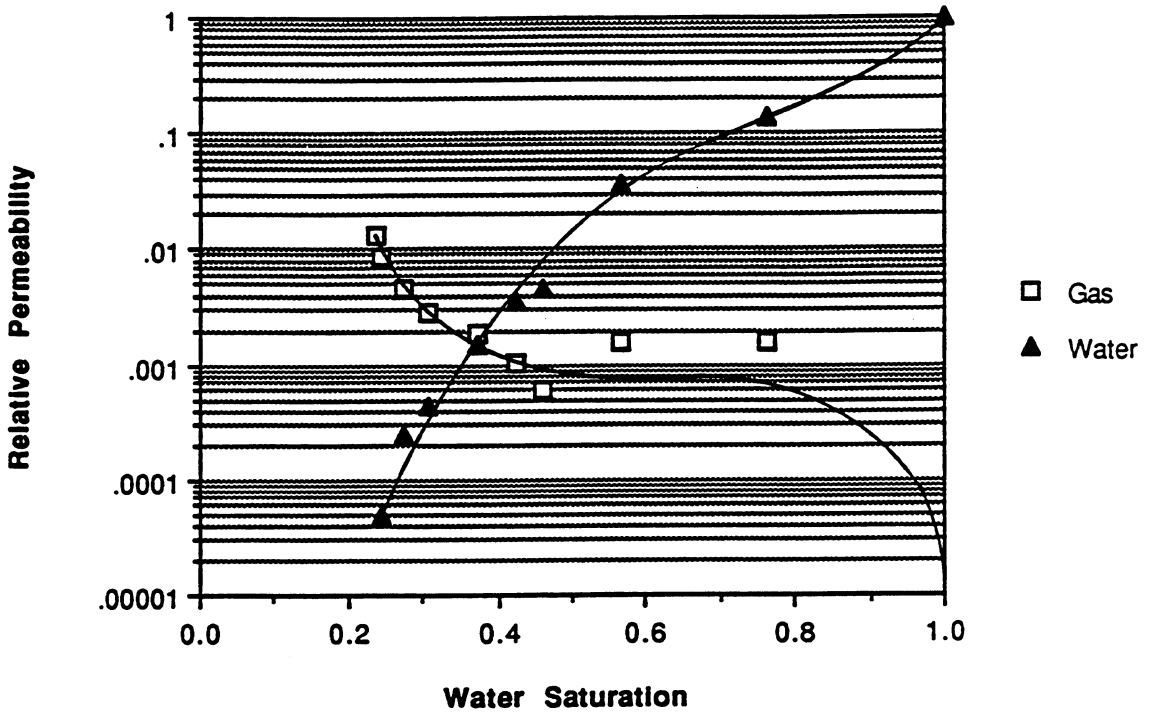

FIGURE 41. - Gas-water relative permeability test no. 4, using foamer at 2.5 psi/ft in a high-permeability core.

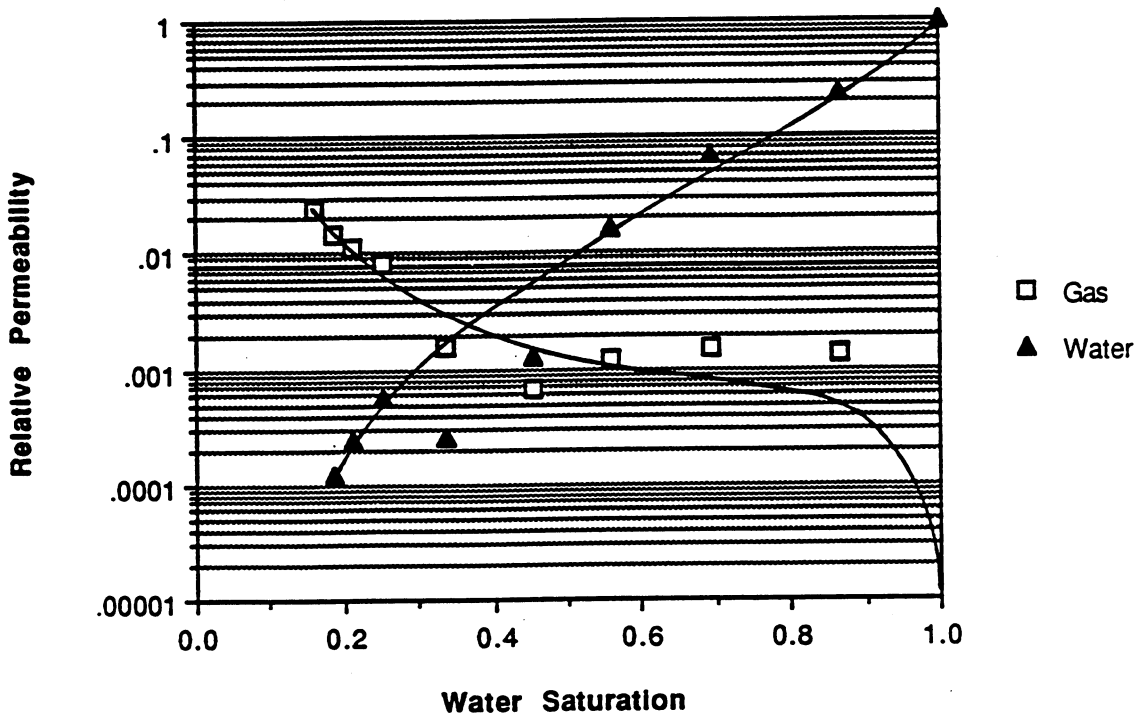

FIGURE 42. - Gas-water relative permeability test no. 5, using foamer at 5.0 psi/ft in a high-permeability core.

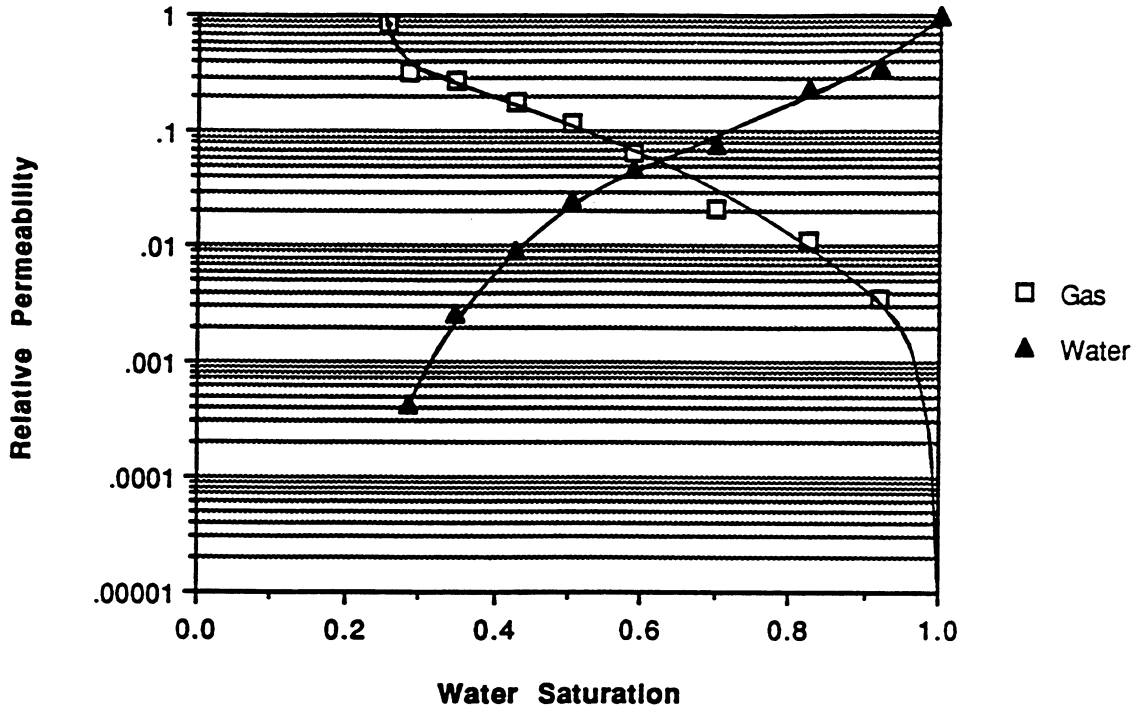

FIGURE 43. - Gas-water relative permeability test no. 6, using brine at 5.0 psi/ft in a high-permeability core.

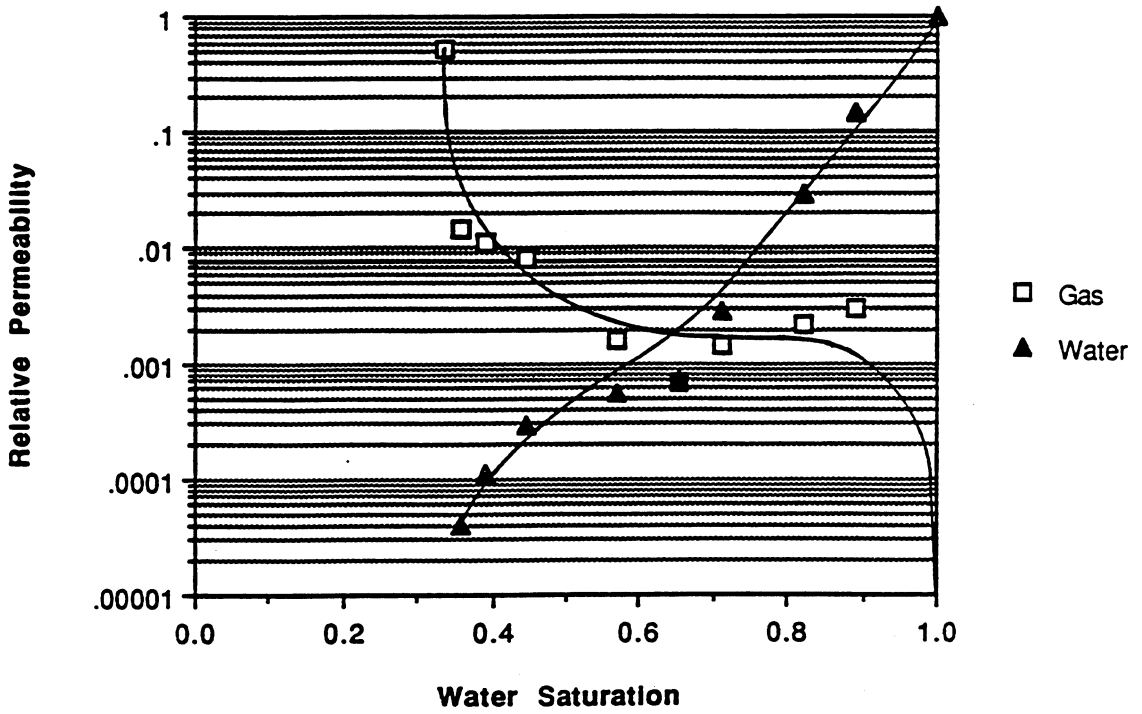

FIGURE 44. - Gas-water relative permeability test no. 7, using brine at 2.5 psi/ft in a high-permeability core.

velocity of the gas, as shown in table 6. The differences due to changing core absolute permeabilities with foamer at the higher differential pressure can be seen by comparing figures 39 and 42 (tests 4 and 5, respectively). Comparison of figures 40 and 43 shows the same effect of core absolute permeability using brine. The effect of absolute permeability was not as great with the foamer as with the brine. Comparing figures 41 and 42 (tests 4 and 5, respectively) shows how the results are affected by changing the pressure differential in the high-permeability core H with foamer. Similarly, comparing figures 43 and 44 (tests 6 and 7, respectively) shows how the pressure differential affected results with brine. The pressure differential effect was slight with foamer, but significant with brine. This may be due to the higher pressure differential's ability to reduce capillary effects, which can hold up high wetting-phase saturations near the ends. The foam serves the same purpose, and provides a more piston-like displacement.

Overall, the permeability to gas was significantly lowered by the foamer, as expected. Table 6 lists the mobility reduction factors due to the presence of the foamer as 0.102 in core E, 0.025 in core H at 2.5 psi/ft, and 0.028 in core H at 5.0 psi/ft. That is, the final relative permeability to gas (and the effective permeability to gas) with foamer at residual water saturation was 10.2, 2.5, and 2.8 % of the value with brine. The reduction was more pronounced in the high-permeability core, which is what other researchers have found.[36,42] This is a possibly favorable aspect of foam behavior, since the foam will reduce the mobility of gas more in the higher-permeability zones of the reservoir, which are the ones most likely to be swept with gas already. Also, the foamer itself will likely enter these zones, allowing the gas to sweep the previously unswept or under-swept lower-permeability zones. This was borne out in results of the previously discussed dual-core experiments.

Shear rates for the six displacements were calculated from the following equation:

$$\text{Shear Rate, sec}^{-1} = 268.4\,(V_f)\sqrt{\frac{\phi \Delta S}{k}} \qquad (19)$$

where V_f = frontal velocity, ft/D

ϕ = porosity, fraction

ΔS = change in displaced fluid saturation, fraction

k = core absolute permeability, md

The resulting calculated shear rates are listed in table 6. Only a small difference in shear rate is noticed between the foamer test (test 2) and the brine test (test 3) in core E, which may explain why the foam did not reduce the gas mobility and relative permeability as much in this low-permeability core as it did in the

high-permeability core. Of course, this shear rate is also a result of the foaming action, since many variables interact with each other.

It could not be positively determined whether the upturn in gas relative permeability at high water saturations with foamer was an artifact of the calculation, or whether it was a real phenomenon occurring in that region of saturation at gas breakthrough and shortly thereafter. During this region, the foam may not be at a high enough quality (high enough gas portion) to reduce the gas relative permeability as low as it could later in the displacement, when the water saturation is lower and foam quality is higher.

The relative permeability data reported herein will be useful for any generic numeric simulations employing similar conditions with the same surfactant. The concept of gathering these data for specific reservoir and injected fluids, and reservoir rock, should be useful to a specific targeted reservoir simulation.

SUMMARY

The following observations were made during the course of this study:

Foam Flow Behavior in Smooth and Packed Capillary Tubes

1. The measured apparent viscosities in the smooth capillary did not significantly depend on surfactant concentrations above the CMC of the system, within the range of concentrations tested (i.e. 0.5 to 2%). Apparent viscosities showed only a slight dependence on temperature. Higher foam qualities resulted in higher measured foam viscosities and yielded larger foam bubble sizes.

2. The dependence of apparent viscosity on shear rate shifted from slightly shear thinning behavior at 60% quality foam to that of sightly shear thickening behavior at foam qualities above 75%. The increase in shear rate also corresponded with a decrease in foam bubble sizes.

3. A mathematical model by Hirasaki and Lawson[20] developed to predict the apparent viscosity of foam in smooth capillaries over predicted the values for the measured apparent viscosity by as much as a factor of 10 at low values of r_B/R. The over-prediction could be attributed to the difference in bubble size distributions between the two studies. Bubble sizes in the present study were considerably smaller than those of the literature data.[20] The model predicted the apparent viscosity becoming increasingly greater as r_B/R approaches zero. This trend may not be correct since as the r_B/R becomes infinitely small, the apparent viscosity should gradually decrease to the value of the surfactant viscosity. The model has to properly account for the variation in r_B/R as it gets smaller.

4. Shear thinning behavior was also observed in experiments conducted in the packed tube indicated by a reduction in the apparent viscosity of the gas in foam as the gas velocity increased.

5. The foam quality in the packed tube study did not have a significant contribution in altering the apparent viscosity of the gas, while the calculated resistance factors increased, almost linearly, with an increase in foam quality. The exponential decay of the the resistance factor as a function of the increase in injection rate was indicative of the shear thinning behavior of this type of foam. Under the conditions tested, the foam achieved a reduced mobility of 0.02 to 0.07 cP^{-1}, an effective viscosity ranging from 14 to 50 cP.

6. The bubble size distribution in the packed tube assembly followed the order: $r/R_{inlet\ section} \geq r/R_{outlet\ section} \gg r/R_{packed\ section}$. Bubble sizes in the packed section were fairly uniform in distribution considering the variation in foam quality and injection rates tested.

7. The extension of the mathematical model to predict the viscosity of gas in foam in the packed tube was used to compare the results of the experimental measurements. Agreement between the values of the measured and predicted viscosities was achieved when the proper ξ_2, weighting factor, was used in the equation. The model for smooth capillary tubes alone under predicted the measured viscosities. The model developed for the smooth capillaries did not over predict the values of the apparent viscosities in the packed tube unlike in the case with the smooth capillary tube primarily because of the difference in the ratios of radii of r_B/r_{cap} (1.38) and r_B/R (0.09). The ratio of the radii in the packed tube were considerably larger than the ones in the smooth capillary tube. The model for smooth capillary tubes failed to correctly predict the cases when the ratio of the radius was less than 0.1.

Effect of Injection Rate on Foam Performance

1. Results of three experiments showed that the higher injection rates of nitrogen displacing the surfactant solution resulted in foam generation that contributed to a significant increase in sustained pressure gradient across the core. Foam bubbles were also observed in the outlet sight glass during the experiment. Fluid injection rates can significantly affect foam behavior.

Effect of Foam on Gas Sweep and Gas-Water Relative Permeability

1. Foams can effectively divert flow of gas from high-permeability, gas-swept zones to low-permeability inadequately swept zones, thereby increasing oil recovery.

2. Using slugs of foamer, as opposed to saturating the rock with foamer, often results in varying, non-equilibrium flow, which may not be predictable.

3. Calculation of gas-water relative permeabilities, with the foamer considered as the water phase, can be useful in understanding of complex foam behavior.

4. Foam is more effective in reducing gas mobility and relative permeability in high-permeability zones, than in low-permeability zones.

5. Foam behavior is highly dependent upon imposed pressure differential, which itself interacts with and is affected by injection rates; injection sequences; saturations; and flowing pore structure.

REFERENCES

1. National Petroleum Council. Enhanced Oil Recovery. Washington, D.C. 1984.

2. Stalkup, F.I., Jr. Miscible Displacement; Monograph Series Volume 8, Society of Petroleum Engineers, Dallas; 1983.

3. Heller, J. P., D. K. Dandge, R. J. Card, and L. G. Donaruma. Direct Thickeners for Mobility Control of CO_2 Floods. Pres. at the SPE Int'l. Symp. on Oilfield and Geothermal Chemistry, Denver, June 1-3, 1983. SPE paper 11789.

4. Dandge, D. K. and J. P. Heller. Polymers for Mobility Control in CO_2 Floods. Pres. at the SPE Int'l Symp. on Oilfield Chemistry, San Antonio, Feb. 4-6, 1987. SPE paper 16271.

5. Terry, R. E., A. Zaid, C. Angelos, and D. L. Whitman. Polymerization in Supercritical CO_2 to Improve CO_2/Oil Mobility Ratios. Pres. at the SPE Int'l Symp. on Oilfield Chemistry, San Antonio, Feb. 4-6, 1987. SPE paper 16270.

6. Llave, F. M., F. T. H. Chung, and T. E. Burchfield. The Use of Entrainers in Improving Mobility Control of Supercritical Carbon Dioxide. Pres. at the SPE/DOE Sixth Symp. on EOR, Tulsa, OK, Apr. 17-20, 1988. SPE/DOE paper 17344.

7. Llave, F. M. Improvement of Gas Mobility Control and Displacement Efficiency by Means of Entrainers. Pres. at the AIChE Tri-Sectional Mtg., Bartlesville, OK, Mar. 11, 1989.

8. Chiang, J. C., S. K. Sawyal, L. M. Castanier, W. E. Brigham, and A. Sufi. Foam as a Mobility Control Agent in Steam Injection Processes. Pres. at the SPE 50th Annual California Regional Meeting, Los Angeles, Apr. 9-11, 1980. SPE paper 8912.

9. Dilgren, R. E., A. R. Deemer, and K. B. Owens. The Laboratory Development and Field Testing of Steam/Noncondensable Gas Foams for Mobility Control in Heavy Oil Recovery. Pres. at the SPE California Regional Meeting, San Francisco, Mar. 24-26, 1982. SPE paper 10774.

10. Albrecht, R. A., and S. S. Marsden. Foam as Blocking Agents in Porous Media. Soc. Pet. Eng. J., March 1970, pp. 51-55.

11. Bernard, G. G., L. W. Holm, and C. P. Harvey. Use of Surfactant to Reduce CO_2 Mobility in Oil Displacement. Pres. at the SPE 54th Annual Fall Mtg., Las Vegas, Sept. 23-26, 1979. SPE paper 8370.

12. Heller, J. P., L. L. Cheng, and M. S. Kuntamukkula. Foamlike Dispersions for Mobility Control in CO_2 Floods. Soc. Pet. Eng. J., August 1985, pp. 603-613.

13. Borchardt, J. K., D. B. Bright, M. K. Dickson, and S. L. Wellington. Surfactants for CO_2 Foam Flooding. Pres. at the 60th SPE Ann.Tech. Conf. and Exhibition, Las Vegas, Sept. 22-25, 1985. SPE paper 14394.

14. Kamal, M., and S. S. Marsden. Displacement of a Micellar Slug Foam in Unconsolidated Porous Media. Pres. at the SPE 48th Annual Fall Mtg., Las Vegas, Sept. 30 - Oct. 3, 1973. SPE paper 4584.

15. Lawson, J. B., and J. Reisberg. Alternate Slugs of Gas and Dilute Surfactant for Mobility Control During Chemical Flooding. Pres. at the 1st SPE/DOE Symp. on Enhanced Oil Recovery, Tulsa, Apr. 20-23, 1980. SPE/DOE paper 8839.

16. Llave, F. M., J. M. Sturm, and D. K. Olsen. Development of Novel EOR Methods: Foams for Mobility Control in Surfactant Flooding. Dept. of Energy Report No. NIPER-369, January 1989.

17. Chung, F. T. H., and D. A. Hudgins. Development of an Engineering Methodology for Applying Foam Technology. U.S. Dept. of Energy Report No. NIPER-374, September 1988.

18. Hirasaki, G.J. The Steam-Foam Process. J. Pet. Tech., May 1989, p. 449.

19. Falls, A. H., P. A. Gauglitz, G. J. Hirasaki, D. D. Miller, T. W. Patsek, and J. Ratulowski. Development of a Mechanistic Foam Simulator: The Population Balance and Generation by Snap-Off. Pres. at the SPE/DOE Fifth Symp. on EOR, Tulsa, Apr. 20-23, 1986. SPE/DOE paper 14961.

20. Friedman, F., W. H. Chen, and P. A. Gauglitz. Experimental and Simulation Study of High-Temperature Foam Displacement in Porous Media. Pres. at the SPE/DOE Sixth Symp. on EOR, Tulsa, Apr. 17-20, 1988. SPE/DOE paper 17357.

21. Hirasaki, G. J., and J. B. Lawson. Mechanisms of Foam Flow in Porous Media: Apparent Viscosity in Smooth Capillaries. Soc. Pet. Eng. J., April 1985, pp. 176-190.

22. Falls, A. H., J. J. Musters, and J. Ratulowski. The Apparent Viscosity of Foams in Homogeneous Bead Packs. SPE Res. Eng. J., May 1989, pp. 155-164.

23. Radke, C. J., and T. C. Ransohoff. Mechanisms of Foam Generation in Glass Bead Packs. SPE Reservoir Engineering, May 1989, pp. 573-585.

24. Ransohoff, T. C., P. A. Gauglitz, and C.J. Radke. Snap-off of Gas Bubbles in Smoothly Constricted Noncircular Capillaries. AIChE J., May 1987, pp. 753-765.

25. Gauglitz, P. A., C. M. St. Laurent, and C. J. Radke. An Experimental Investigation of Gas Bubble Breakup in Constricted Square Capillaries. J. Pet. Tech., Sept. 1987, pp. 1137-1146.

26. Khatib, Z. I., G. J. Hirasaki, and A. H. Falls. Effects of Capillary Pressure on Coalescence and Phase Mobilities in Foams Flowing through Porous Media. SPE Reservoir Engineering, Aug. 1988, pp. 919-926.

27. Shirley, A. I. Foam Formation in Porous Media, A Microscopic Visual Study. In Surfactant-Based Mobility Control. D. H. Smith (ed.), ACS Sym. Series 373, American Chemical Soc., Washington, D.C., 1988, pp. 234-257.

28. Kuehne, D. L., D. I. Ehman, A. S. Emanuel, and C. F. Magnani. Design and Evaluation of a Nitrogen Foam Field Trial. Pres. at the SPE/DOE Sixth Symp. on EOR, Tulsa, OK Apr. 17-20, 1988. SPE/DOE paper 17381.

29. Patton, J. T. Enhanced Oil Recovery by CO_2 Foam Flooding. Dept. of Energy Report No. DOE/MC/03259-15, April 1982.

30. Heller, J. P., and J. J. Taber. Development of Mobility Control Methods to Improve Oil Recovery by CO_2. U.S. Dept. of Energy Report No. DOE/MC/10689-17, November 1983.

31. Gao, H. W. Design, Construction, and Operation of an Apparatus To Measure Viscosity and Screen Factor of Polymer Solutions at High Temperatures. Dept. of Energy Report No. NIPER-221, November 1986.

32. Rabinowitsch, B. Ueber die Viskositat and Elastiziitat Von Solen. Z. Physik. Chem. A145, 1-26, 1929.

33. Bird, R. B., W. E. Stewart, and E. N. Lightfoot. Transport Phenomena; John Wiley and Sons, New York, 1960.

34. Marsden, S. S., and S. A. Khan. The Flow of Foam Through Short Porous Media and Apparent Viscosity Measurements. Soc. Pet. Eng. J., March 1966, pp. 17-25.

35. Minssieux, L. Oil Displacement by Foams in Relation to Their Physical Properties in Porous Media. J. Pet. Tech., January 1974, pp. 100-108.

36. Raza, S. H. Foam in Porous Media: Characteristics and Potential Applications. Soc. Pet. Eng. J., Dec. 1970, pp. 328-336.

37. Gao, H. W., P. B. Lorenz, and S. Brock. Rheological Behavior of Pusher 500 under a Variety of Chemical and Thermal Conditions. Dept. of Energy Report No. NIPER-225, February 1987.

38. Jennings, R. R., J. H. Rogers, and T. J. West. Factors Influencing Mobility Control by Polymer Solutions. J. Pet. Tech., March 1971, pp. 391-401.

39. Huh, D.G. and L.L. Handy. Comparison of Steady- and Unsteady-State Flow of Gas and Foaming Solution in Porous Media. SPE Reservoir Engineering, February 1989, pp. 77-84.

40. Jones, S.D. and W.O. Roszelle. Graphical Techniques for Determining Relative Permeability from Displacement Experiments. J. Pet. Tech., May 1978, pp. 807-817; Trans., AIME, 265.

41. Johnson, E.F., D.P. Bossler and V.O. Naumann. Calculation of Relative Permeability from Displacement Experiments. Petroleum Transactions, AIME, v.2 16, 1959, pp.370-372.

42. Mast, R. F. Microscopic Behavior of Foam in Porous Media. Pres. at the SPE 47th Annual Fall Meeting, San Antonio, Oct. 8-11, 1972. SPE paper 3997.

☆U.S. GOVERNMENT PRINTING OFFICE: 1989-761-030/00059